TOTAL SUSPENDED PARTICULATE MATTER MAPPING USING LANDSAT 7 ETM AND MODIS AQUA: MAHAKAM DELTA CASE STUDY

ANIQ FADHILLAH
MARCH, 2011

SUPERVISORS:
Dr. Zoltán Vekerdy
Prof. Dr. Ing. Wouter Verhoef

ADVISOR:
Syarif Budhiman

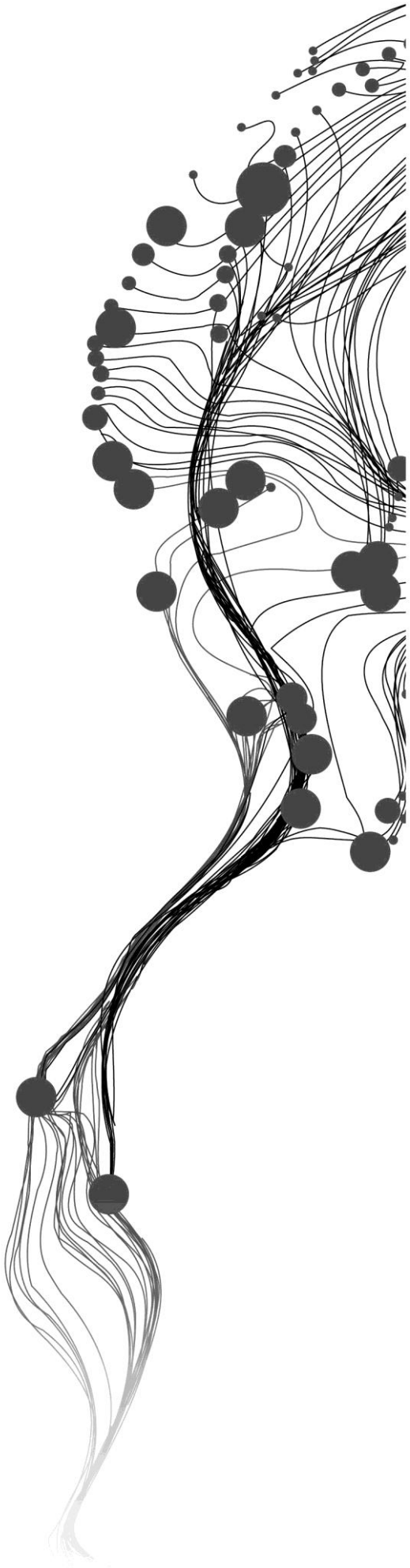

TOTAL SUSPENDED PARTICULATE MATTER MAPPING USING LANDSAT 7 ETM AND MODIS AQUA: MAHAKAM DELTA CASE STUDY

ANIQ FADHILLAH
Enschede, The Netherlands, March, 2011

Thesis submitted to the Faculty of Geo-Information Science and Earth Observation of the University of Twente in partial fulfilment of the requirements for the degree of Master of Science in Geo-information Science and Earth Observation.
Specialization: Water Resources and Environment Management

SUPERVISORS:
Dr. Zoltán Vekerdy
Prof. Dr. Ing. Wouter Verhoef

ADVISOR:
Syarif Budhiman

THESIS ASSESSMENT BOARD:
Dr. Ir. Chris Mannaerts (Chair)
Dr. D.M. Harper (External Examiner, Department of Biology - University of Leicester - UK)

ABSTRACT

This study is part of the water quality research carried out in the Mahakam Cluster of the East Kalimantan Project. Look up tables were constructed from a water optical model.. These were used for the mapping of water quality parameters from LANDSAT 7 ETM and MODIS daily reflectance (MOD09GA/ MYD09GA) images.

For validation, the TSM maps derived from MODIS were compared to field data and in addition the TSM maps derived from LANDSAT 7 ETM and MODIS TERRA were compared with each other.

In situ TSM concentration field measurements and TSM concentrations derived from MODIS daily reflectance image show a good correlation. This appears from the type II regression analysis result, R^2 =0.87, RMSE = 0.147 and R^2 =0.97, RMSE=0.0895 both for AQUA and TERRA, respectively. From this result it can be concluded that look up tables can be used to derive TSM concentration from remote sensing imagery.

Comparing a TSM MAP derived from LANDSAT ETM and one from MODIS TERRA, the result is a low correlation with R^2 = 0.21 and RMSE = 0.468. The TSM map concentration derived from LANDSAT 7 ETM is underestimated compared to the TSM concentration from MODIS TERRA. Further studies need to be carried out to investigate this discrepancy.

Keywords: TSM, Mahakam Delta, LANDSAT 7 ETM, MODIS AQUA (MYD09GA), MODIS TERRA (MOD09GA), Look up Table.

ACKNOWLEDGEMENTS

Alhamdulillahi Rabbil'alamin.

No other word could express my gratitude to Allah S.W.T. The Merciful so that I am able to accomplish my work which I dedicate to my beloved parents, *abah* Mohammad Natsir, *mimi* Maskuroh, and my sister, *dek* Istnaini Zulaikha Rahmadhani.

This piece of work would not be readable without help of many people. I would like to convey my appreciation to Dr. Zoltan Vekerdy as my first supervisor for his patience and guidance, my second supervisor, Prof. Dr. Ing. Wouter Verhoef for his advices, Dr. Ir. M.M. Chris Mannaerts as member of my assessment board, and not to forget my advisor, Syarif Budhiman, for his continous support.

I also would like to thank lecturers and staffs of ITC Faculty of Twente University, especially those in the Water Resources and Environment (WREM) Department for their knowledge contribution, support and friendship during my study in WREM Department. Thank you to all of my friends for nice memories and supports.

This study would not be complete without in-situ data from my advisor and image data which is accessed freely. These image data are distributed by the Land Processes Distributed Active Archive Center (LP DAAC), located at the U.S. Geological Survey (USGS) Earth Resources Observation and Science Center (EROS) (lpdaac.usgs.gov).

The last, this Master of Science study would not be happened without funding from The Joint Japan World Bank Graduate Scholarship Program (JJ/WBGSP). Thank you for the opportunity.

Enschede, 21 February 2011

Aniq Fadhillah (Ms.)

TABLE OF CONTENTS

LIST OF FIGURES

LIST OF TABLES

1. INTRODUCTION

Total Suspended Matter (TSM) or total suspended solid (TSS) can be identified as particulate matter in water column which has size equal or larger than 0.45 micron (Ouillon et al., 2008). TSM in water bodies play a vital role in the quality and dynamics of the estuarine and coastal environments. All natural water bodies contain suspended matter which consists of organic and inorganic matters. (Pozdnyakov & Grassl, 2009). Extreme chlorophyll-a and TSM concentration in water body will affect the plankton primary production (Hommerson, 2009) and the thermodynamic stability of coastal waters. It also can affect the visibility in the water (Davies-Colley & Smith, 2001) and become a limiting factor for aquatic ecosystems (Ambarwulan, 2002).

Previously, aquatic ecosystem quality was monitored by using conventional ways which only depend on in situ measurements. Large extent of water bodies and other practical barriers have become a limitation on conducting extensive and periodical water quality monitoring. At present, this limitation could be overcome by utilizing remote sensing data. This is because remote sensing data offers wider area coverage and possibility for frequent data acquisition (Budhiman, 2004; Salama & F, 2009). Furthermore, remote sensing is valuable particularly when the monitored area is inaccessible or at restricted area (IOCCG, 1998). Information on suspended and dissolved material in a water body is acquired by detecting the upwelling electromagnetic energy from the water surface (Sturm, 1981) captured by a sensor of a remote sensing satellite.

Earlier studies have proven that TSM concentration can be retrieved using remote sensing data. Studies on suspended sediment retrieval using remote sensing data, especially in Indonesian coastal waters, have been conducted using SPOT, ASTER, AVHRR, SeaWiFS and LANDSAT TM data (Abu Daya, 2004; Ambarwulan, 2002; Budhiman, 2004). However the repetition of remote sensed data (temporal resolution) is inadequate to observe its dynamic in most coastal waters (Miller, McKee, & D'sa, 2007).

1.1. Research Problem

Indonesia lies between two oceans and continents, has a wide coastal and ocean area with very dynamic changes. Coastal development in Indonesia has become a major study in the past years due to its rapid development. Coastal development decision makers need more reliable data about coastal dynamics in order to make better decisions. This could be obtained from remote sensing data. Mahakam Delta has similar problems as other coastal areas such as land conversion in the upstream areas, which leads to the increase of sediment load in the delta (Budhiman, 2004).

Remote sensing has two important characteristics, among others: spatial and temporal resolution. LANDSAT can provide detailed information, due to its spatial resolution. However, the temporal resolution of LANDSAT limits its ability to provide dynamic information. To address this limitation, better temporal resolution is needed. In this study, MODIS is chosen in order to provide more frequent temporal data. Both data could complement each other to provide better information on coastal and ocean dynamic around Mahakam delta.

1.2. Objectives

This study is part of the water quality research carried out in the Mahakam Cluster of the East Kalimantan Project supported by the Foundation for the Advancement of Tropical Research (WOTRO) Royal Netherlands Academy of Arts and Sciences (KNAW).

1.2.1. Main Objectives

The main objective of this study is to map TSM concentration distribution using LANDSAT 7 ETM, MODIS MOD09GA and MODIS MYD09GA using look up table developed by Syarif Budhiman (in-preparation).

1.2.2. Sub Objectives

To derive TSM map from

a. LANDSAT 7 ETM
b. MODIS AQUA MYD09GA
c. MODIS TERRA MOD09GA

1.3. Research Questions

1. Is there any different TSM concentration from MODIS AQUA/TERRA and TSM in situ measurement?
2. Is there any different of TSM concentration from LANDSAT 7 ETM and MODIS AQUA?

2. WATER COLOR REMOTE SENSING

A passive system of water colour remote sensing utilizes a narrow field of view sensor. The sensor has to have capability to monitor the radiometric flux at several particular wavelengths in the visible and near infra-red electromagnetic spectrum. The sensor depends on the sun as its energy source (Sathyendranath, 2000).

2.1. Water Colour Remote Sensing Imageries for Water Quality Monitoring

Remote sensing technology has drawn extensive applications in water quality monitoring, especially after the launch of the first ocean colour satellite in 1978 with the launched of Coastal Zone Colour Scanner (CZCS). Although it was only operated for eight years, CZCS has opened a new stage of ocean colour observation (IOCCG, 1998).

After that, many countries contributed to ocean colour sensor development. Following the end of the operation of CZCS in 1996, three ocean-colour sensors were launched. Japan contributed with its Ocean Colour and Temperature Sensor (OCTS), France with its POLarization and Directionality of the Earth's Reflectances (POLDER), and then Germany with the Moderate Optoelectrical Scanner (MOS). Those three sensors only operated in short periods. Post to that, Office of Space Communication National Aeronautics and Space Administration (OSC NASA) launched SeaWiFS in 1997 (IOCCG, 1998).

Ocean colour remote sensing is based on the electromagnetic energy of 400-910 nm wavelengths. The energy is emitted by the sun, transmitted through the atmosphere, reflected by the water body, transmitted by the atmosphere and recorded by the sensor. The photons of the incoming light from the sun follow different paths before hitting the sensor (Sathyendranath, 2000). They undergo collisions with aerosol particles and air molecules on their way throughout the atmosphere. The photons are either absorbed or scattered as a consequence of these collisions. The captured light carries important information (Sathyendranath, 2000).

Sathyendranath (2000) shows important factors influencing the light which interacts with a water body and captured by a sensor in Figure 1. Those factors are: light scattering by suspended matters (a), light scattering by water molecule (b), light absorption by colour dissolved organic matter (c), bottom reflectance (d), and light scattering by phytoplankton (e). The organic and inorganic water constituents are responsible for the water colour (Morel, 1980) which can be characterized by water quality parameters (Pozdnyakov & Grassl, 2009). However, the atmospheric effects and water body's specular reflection generate noise and need to be corrected in order to produce correct water colour information. This process is generally known as atmospheric correction.

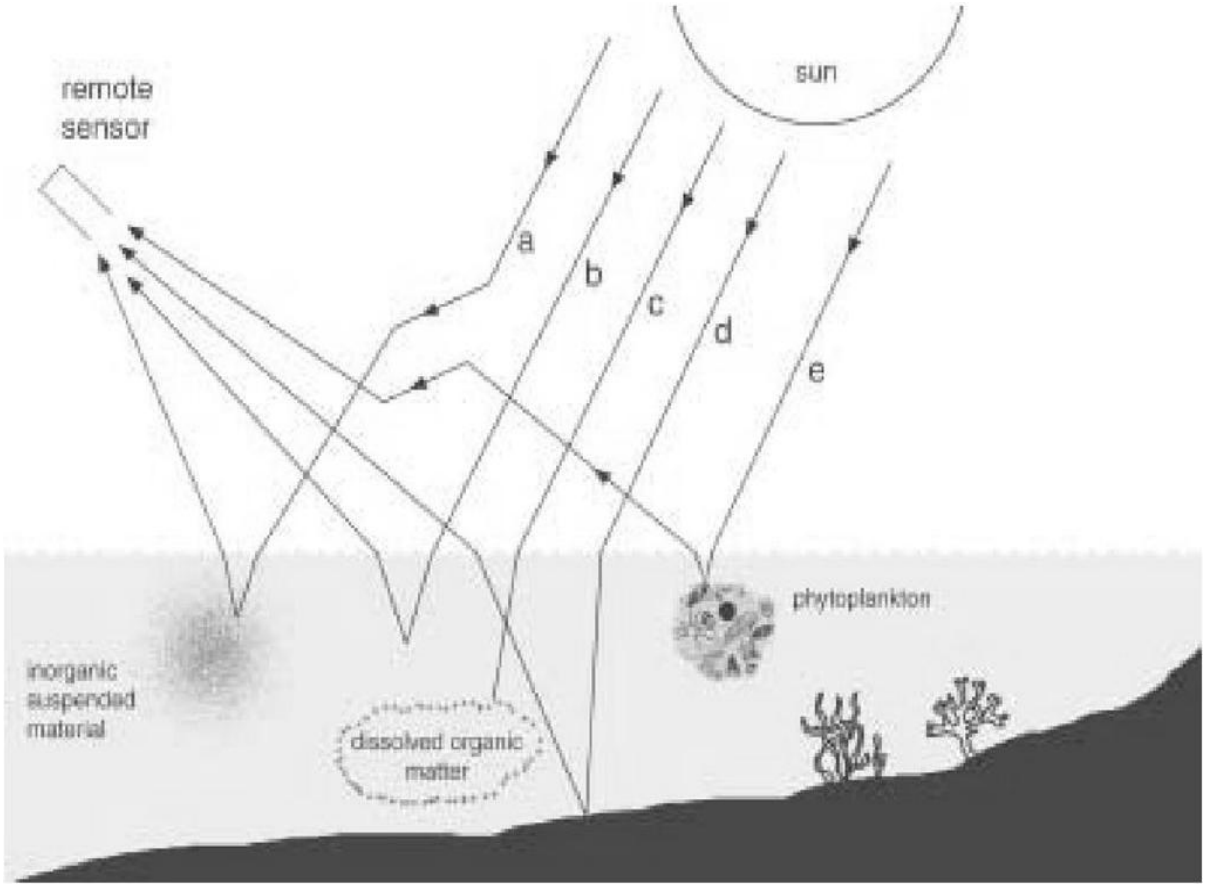

Figure 1. Factors which influence light interaction from water body captured by sensor (Sathyendranath, 2000)

2.2. Atmospheric Correction

The purpose of atmospheric correction for the remote retrieval of ocean properties is to remove the atmospheric and surface effects from the signal measured by the satellite-sensor, resulting in the reflectance coming from the water bodies (IOCCG, 2010). The atmospheric effects can be calculated and removed. However, this can be done when additional measurements are made (IOCCG, 1998).

The atmosphere mainly consists of a mixture of gases. Some of these gases are relatively stable and some are varies in concentration. Nitrogen and oxygen dominate the stable gases, while water vapour and ozone dominated the variable ones. Aerosols are also present in the atmosphere. Those absorb and scatter light. The light that reaches the water surface is modified from what reached the top of the atmosphere (TOA) (Zaneveld, Twardowski, Barnard, & Lewis, 2005).

The TOA reflectance $\rho_t(\lambda)$ can be partitioned linearly into various distinct physical contributions (Gordon & Wang, 1994):

$$\rho_t(\lambda) = \rho_r(\lambda) + \rho_a(\lambda) + \rho_{ra}(\lambda) + \rho_g(\lambda) + t\rho_w(\lambda) \quad \text{Equation 1}$$

Where ρ_t is total reflectance; ρ_r is Rayleigh scattering effect; ρ_a is aerosol scattering effect; ρ_{ra} is interaction between molecular and aerosol scattering; ρ_g is solar beam reflectance; ρ_w is water reflectance and t is air transmittance (Gordon & Wang, 1994).

The radiative transfer is now well understood and accurately modelled. The Simulation of Satellite Signal in the Solar Spectrum (5S) models the radiative transfer in clear atmosphere. It calculates how the Earth-atmosphere affects the sun radiation that is backscattered to the satellite altitude in different illumination-observation situations. It takes into account gaseous absorption effects, molecule and aerosol scattering and spatial in homogeneities on the surface reflectance. However, this model is reported as too expensive and time consuming to be used on an operational basis. A simple model developed from this radiative transfer model is SMAC. The Simplified Method for Atmospheric Correction (SMAC) is developed to overcome 5S weakness (Rahman & Dedieu, 1994).

2.3. Water Constituent Interaction on Water

As it was mentioned above, certain organic and inorganic water constituents are responsible for water colour (Morel, 1980). Those constituents are chlorophyll-a (Chl-a) in the phytoplankton, suspended particulate matter (TSM), and coloured dissolved organic matter (CDOM). Each constituent has specific reaction with the incoming light, i.e. absorption and scattering. They has its own scattering and absorption characteristics, which are wavelength dependent (Sturm, 1981).

Figure 2. Water Colour from LANDSAT ETM acquired on 11 January 2007 with 3-2-1 band combination at Mahakam Delta, Indonesia.

Red arrows on Figure 2 show different water colours, which are governed by water constituents. The sunlight is not merely reflected from the water surface. The colour of water surface are results from sunlight that has entered the water, been selectively absorbed, scattered and reflected by water, phytoplankton and other suspended and dissolved materials in the upper layers, and then backscattered through the surface.

2.3.1. Water

Aquatic environment can be subdivided according to whether the natural water body is salty (oceanic), inland or fresh, or coastal (Pozdnyakov & Grassl, 2009). Apart from those distribution, each water body is categorized into case-1 or case-2 waters, which refers to ocean or turbid shallow waters, respectively, based on whether they contain suspended matter or not. Water as a media has its special absorption and scattering characteristic. Pop and Fry (1997) have analysed documented water absorption. Their result on the pure water scattering is shown in Figure 3 and absorption coefficient is shown in Figure 4. Overall water absorption coefficient which is used in this study can be found in Appendix section B.

From Figure 4, it is shown that the absorption of pure water is the lowest at the short and middle wavelength of the visible range. The pattern shows a continuous increase in the absorption at λ>500nm. IR absorption at λ>700nm is more intense compared to the absorption in the red band.

Water scattering properties are generally influenced by the Rayleigh scattering mechanism (Pozdnyakov & Grassl, 2009).

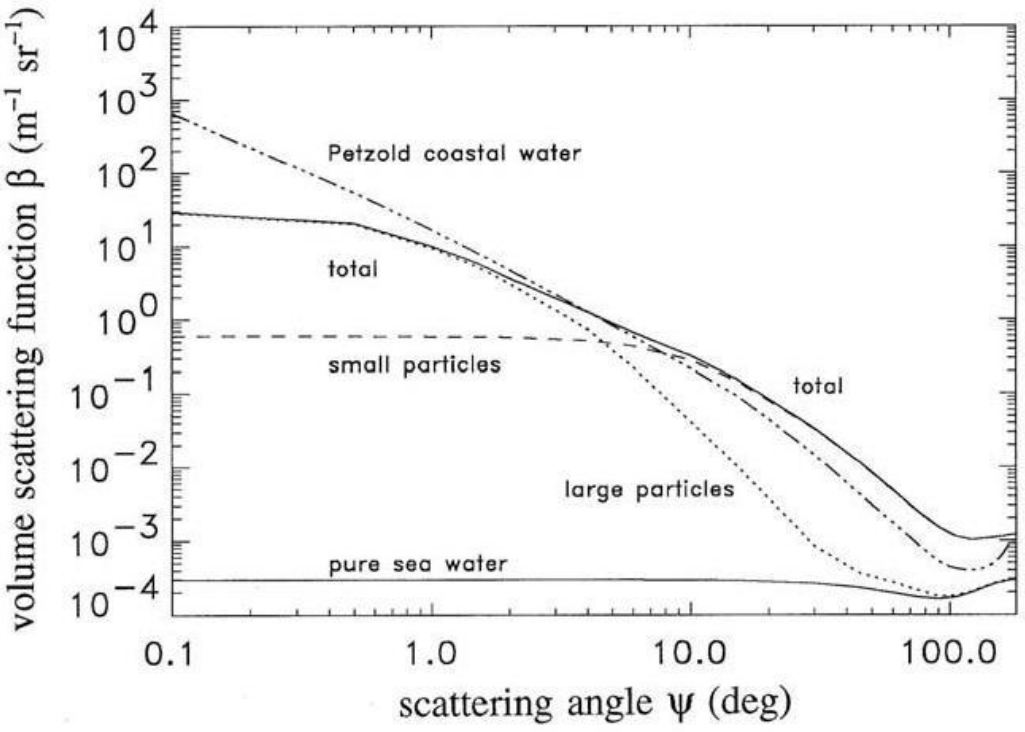

Figure 3. Comparison of volume scattering function by Kopelevich model and Petzold measurement (Mobley, 2004)

2.3.2. Phytoplankton

Sathyendranath (2000) describes phytoplankton as ubiquitous, microscopic, free-floating organisms found in the illuminated surface layers of a water body. It is acknowledged as the most important constituent responsible for variations in the optical properties of water body. It is known that phytoplankton specific absorption is related to chlorophyll-a concentration (Bricaud, Babin, Morel, & Claustre, 1995; Cleveland, 1995). Figure 4 shows that generally strong absorption is shown in blue band and in red band (Sathyendranath, 2000).

Phytoplankton absorption parameters can be parameterized below (D'sa & Miller, 2005; Morel, 1980):

$$a_{phy} = a^*_{phy} * Chl$$ Equation 2

Where a^*_{phy} is phytoplankton specific absorption; and Chl is phytoplankton concentration [mg l^{-1}].

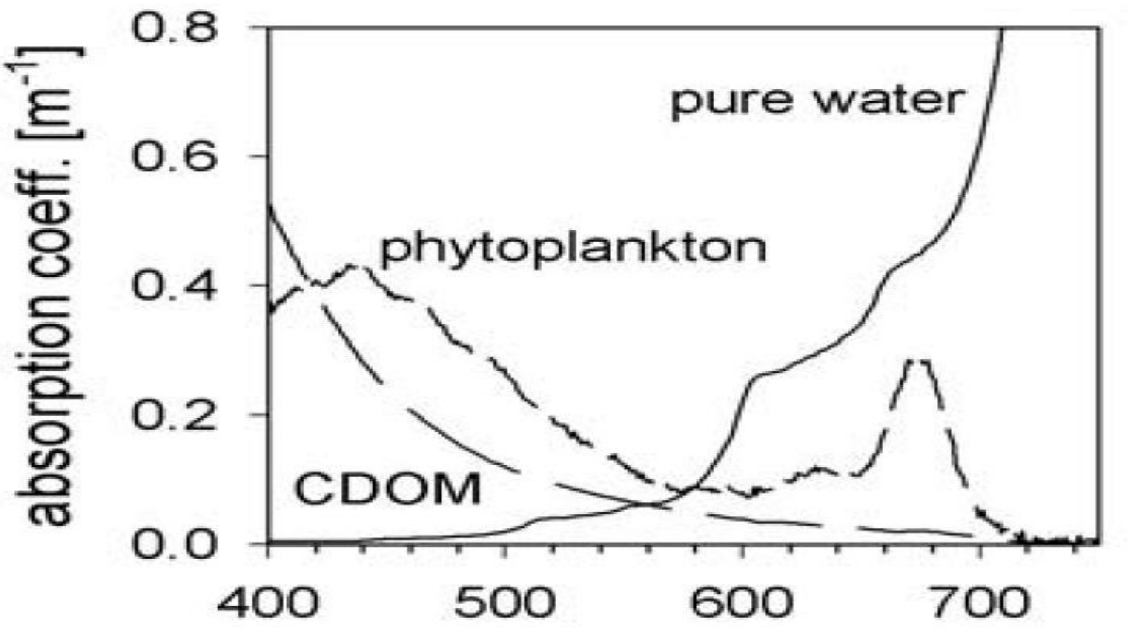

Figure 4. Pure water, phytoplankton and CDOM absorption coefficient (D'sa & Miller, 2005)

2.3.3. Total Suspended Matter (TSM)

Total suspended matter concentrations in coastal and inland surface water bodies can be fairly high (Pozdnyakov & Grassl, 2009). It is influenced by wave and current movement which could carry bottom sediments into suspension, and significantly modify the water colour.

TSM plays an important function in water quality management. It is related to total primary production of both benthic photosynthetic organisms and pelagic to organic micro-pollutants, flux heavy metals, and other anthropogenic materials. TSM concentrations also can be used to monitor turbid river plumes or observing re-suspension of bottom sediments in shallow waters due to tidal action, wind and waves.

Numerous contaminants; organic and heavy metals, adsorb strongly to fine sediments. Thus make sediment act as carrier and also serves as media to remove it from the water column (IOCCG, 2000).

2.3.4. CDOM

Coloured dissolved organic matter (CDOM) is also known as yellow substances or gelbstoff are group of organic, dissolved substances, consisting of humic and fulvic acids (Sathyendranath, 2000).

In area where the land discharge is important, e.i: coastal and inland waters, CDOM obviously a main factor in shifting the water colour, thus, CDOM absorption should be considered as one of total absorption parameter. CDOM absorption can be parameterized below:

$$a_{CDOM} = a^*_{CDOM} * CDOM_{440} \quad \text{Equation 3}$$

Where a^*_{CDOM} is coloured detritus gelbstoff specific absorption; $CDOM_{440}$ is coloured detritus gelbstoff concentration at 440 nm wavelength [mg l^{-1}].

3. MAHAKAM DELTA

The Mahakam delta is located in the eastern central area of the Kalimantan Island (Borneo) Indonesia, between 0°21' and 1°10' Southern latitude, and 117° 15' and 117°40' Eastern longitude. Administratively, Mahakam delta is under Kutai Kertanegara Regency, East Kalimantan Province (Bappeda Kabupaten Kutai Kartanegara, 2007) which consists of 5 districts: Samboja, Sanga-sanga, Muara Jawa, Anggana and Muara Badag. Anggana and Muara Jawa are the areas which situated in Mahakam Delta area (Sandjatmiko, 2006). The largest river in this regency is Mahakam River with 920 Kilometre length (Bappeda Kabupaten Kutai Kartanegara, 2007). This river builds the Mahakam delta. Mahakam delta coastline borders the Makassar Strait (Allen, Laurier, & Thouvenin, 1976).

Figure 4. Map of Indonesia with the Mahakam Delta indicated with the small box
(Source: http://geography.about.com/library/cia/ncindonesia.htm)

The Mahakam Delta as a unique ecosystem has attracted many scientists to gain knowledge of it. It is an active delta system (Allen, et al., 1976). Its development has started from the last phase of the Holocene transgression through sedimentation process (Sandjatmiko, 2006).

3.1. General Morphology

Allen et al. (1976) has documented the morphology of Mahakam delta. Mahakam delta has a very regular fan shape, with distributaries radiating out from the apex at Sanga-sanga or Muara Jawa (Figure7). Three major distributaries spread out from this point to the Northeast, Southeast, and South. These three

distributaries further broaden into second and third order distributaries systems. At the end the fluvial discharge is split into 9 distributaries.

The Mahakam delta consists of distributaries (or river channels), which pass through the delta plain, tidal channels which are open towards the sea at their lower end and usually do not have a permanent connection to the river system, and muddy swamps between the fluvial and tidal channels (Allen & Chambers, 1998).

The distributaries are relatively rectilinear and except at the inlets, they have constant width. The channel thalweg, the line of deepest water part of the river, are meander within the channel. The channel cross sections show the asymmetric contour characteristic of meandering rivers. Channel depths are varies from 5 to 15 meters. The inlets show an estuarine morphology, with channel islands channel bars, and tidal flats (Allen, et al., 1976).

Tidal channels show broadly flaring trumpet shape inlets. Their width is shorter rapidly upstream. These tidal inlets divide upstream into many meandering tidal channels. Tidal channels are much deeper and they can reach 20 meters deep. Tidal channel are rarely connect to fluvial distributaries system (Allen, et al., 1976).

3.2. Tide and tidal Processes

Mahakam delta is located in an area which is under low wave–energy, large tidal amplitude, and large fluvial input. The tides are semi-diurnal with significant diurnal variation. These tides are sufficient to reverse the flow direction of the Mahakam River upstream as far as Samarinda, which is located approximately 20 Km from the delta apex (Mandang & Yanagi, 2007).

Tidal processes is responsible on sediment distribution in the delta mouth (Allen, et al., 1976). Tidal amplitude which is occur every 15-day, are ranging from 0.2m to about 0.6m during spring tide (Allen & Chambers, 1998). Sandjatmiko reported that tidal amplitude in Mahakam River could reach 2.5m high (2006).

The sedimentation processes in the delta plain and on the delta front are strongly influenced by tidal currents (Allen, et al., 1976).

3.3. Ecosystem

Estuarine ecosystem at Mahakam Delta is diverse. 20 species of seven mangroves families are recorded. This is due to fresh water and salty water integration which makes the Mahakam Delta become an ideal place for Mangrove habitat (Sandjatmiko, 2006). *Nypa* palm swamps also can be found here (Storms, Hoogendoorn, Dam, Hoitink, & Kroonenberg, 2005). Mammals, such as monkey is endemic in this area. 125 fish species and shellfish also identified in Mahakam Delta.

Mangrove deforestation in Mahakam delta has broadly reported. Approximately 63% of Mangrove had been converted into shrimp ponds in 2001. This conversion invites erosion and abrasion on the surface

land of the delta. Due to the erosion and abrasion, sedimentation would occur in the river bed or at the front of the delta. The distributaries channel depth would be shallower and the front delta will probably become wider and shift forward (Sidik, 2009).

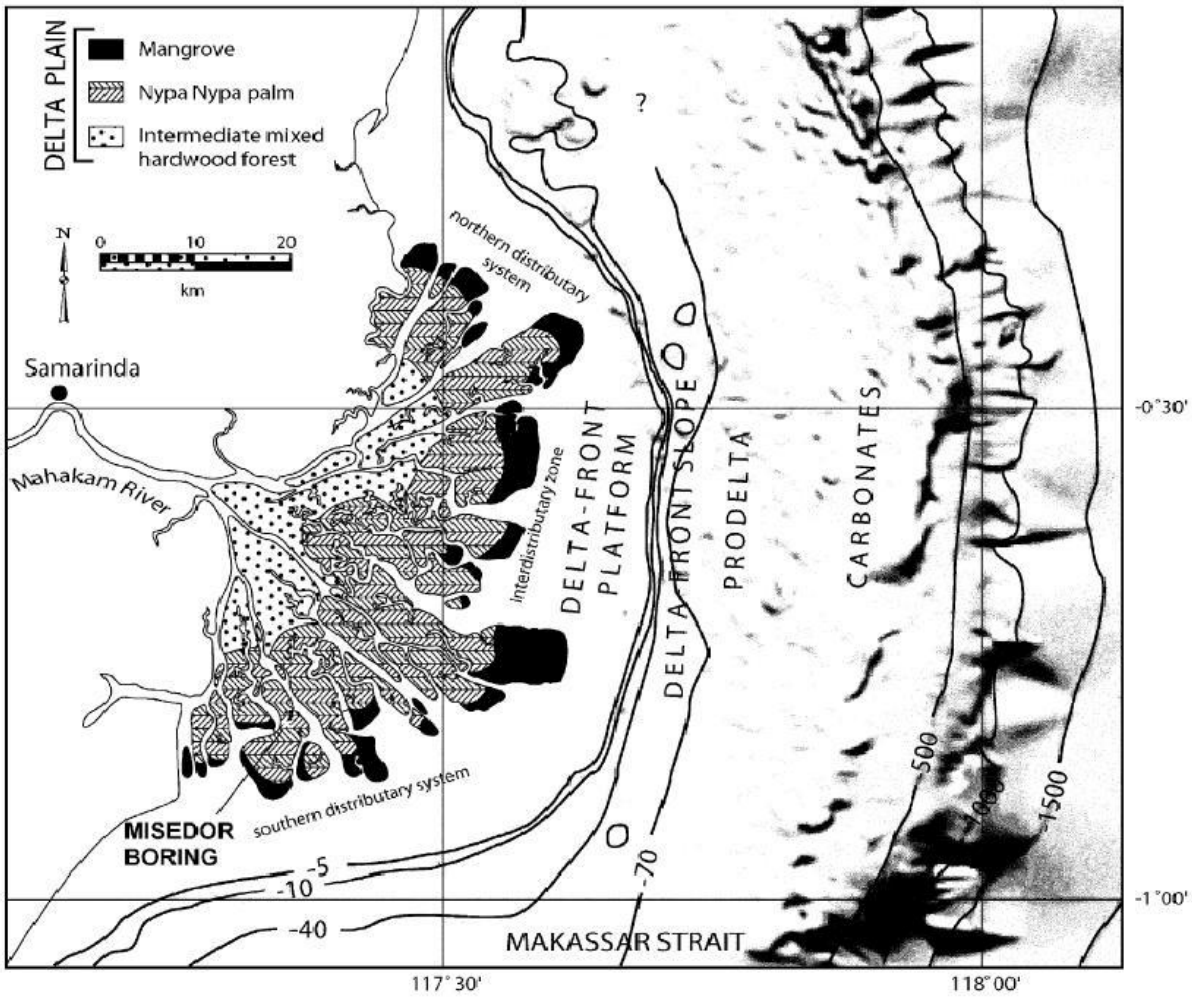

Figure 5. Map of Vegetation zone in Mahakam Delta (Storms, et al., 2005) Contour in meters.

3.4. Climate

Indonesia is affected by the Asian-Australian (AA) monsoon. The southeast monsoon occurs from April to October; whilst the northwest monsoon occurs from November to March. The southeast monsoon carries warm and dry air from Australia. The Northwest monsoon is related with moist and warm air. Wet season starts from October until May and dry season is start from July to September (Ambarwulan, 2010). Indonesia is characterized as Af climate type which describe as tropical rainforest (Peel, Finlayson, & McMahon, 2007). This means that temperature in Indonesia for a whole year is above 18°C, based from the weather database, it was recorded that the temperature are ranging from 24-25°C to 30-31°C with average around 27-28°C (WeatherUnderground, 1991). Therefore there is no such a big different between dry and wet season.

The high temperature and Indonesian location which 70% covered by water area is causing high humidity. High humidity and high temperature is a good combination to form clouds. This is why Indonesia area always covers with clouds.

Rainfall ranges in Mahakam delta area is about 2000 to 3000 mm per year which indicate that river discharge at Mahakam River on the order of 1000 to 3000 cubic m sec^{-1} (Allen, et al., 1976).

3.5. Ocean Water Current

Ocean water is in constant motion. Wind forces currents on the ocean surface. Indonesian archipelago is lies between the Indian and the Pacific Oceans. Mahakam delta has border with Makassar straits. From Figure 6, it can be seen the current direction occur around Mahakam delta and Makassar straits. This current may affect sediments distribution in Mahakam Delta especially around tidal channel.

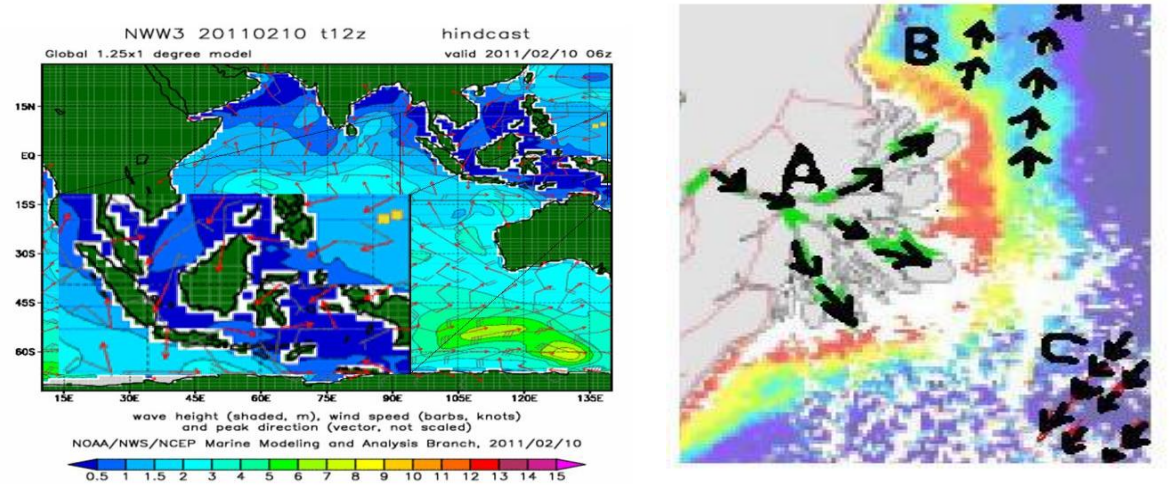

Figure 6. Left Figure: Indonesian Ocean Wave height, Wind Speed and Peak Direction generated from NOAA WAVEWATCH III Model (NOAA, 2010), Right Figure: Mahakam Delta Current direction, (A) From Mahakam river, (B) Northward direction during around December to March, and (C) Southward direction which occurred for a whole year (Abu Daya, 2004).

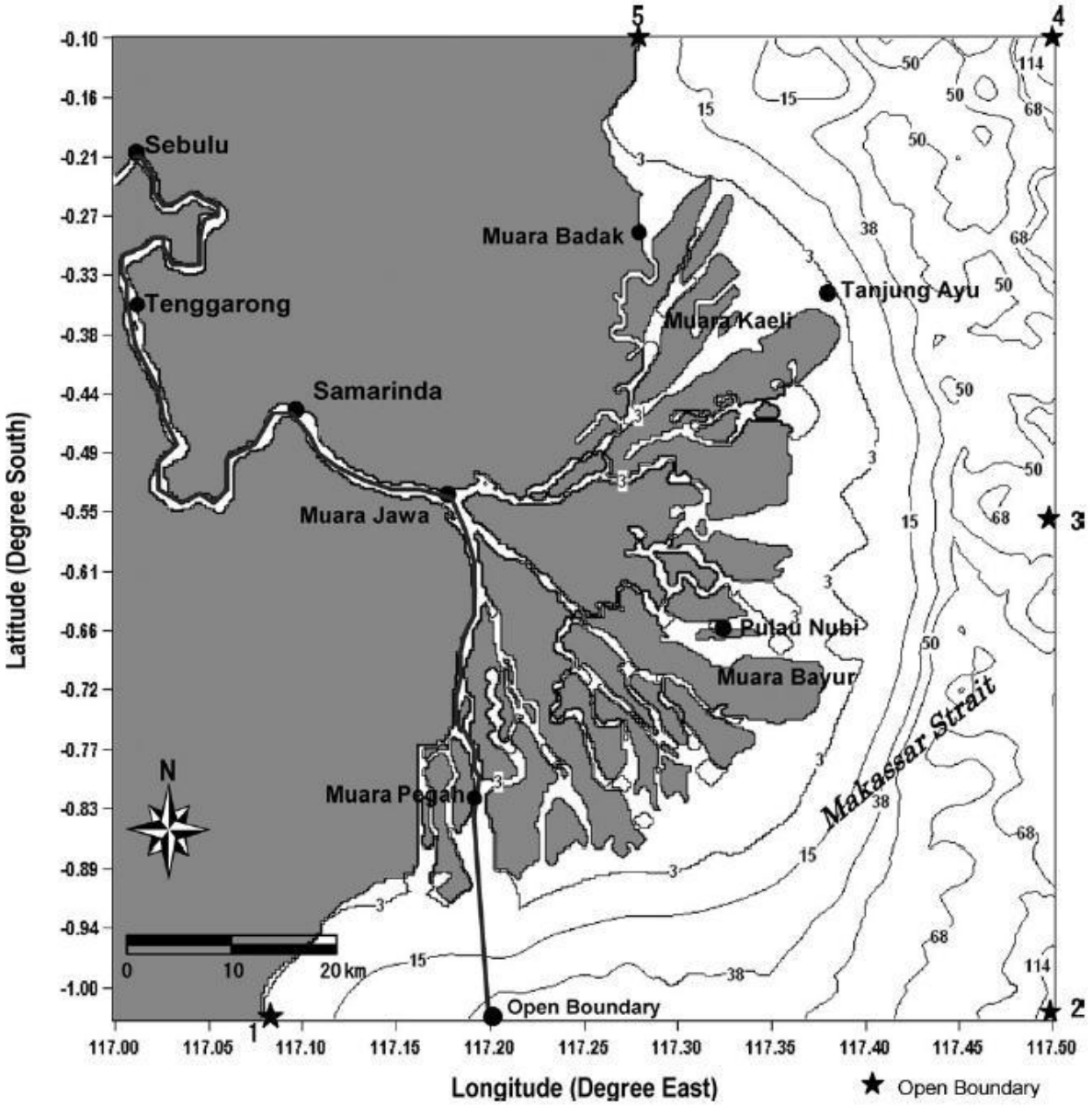

Figure 7. Bathymetric map of the Mahakam estuary from DISHIDROS, Indonesian Navy (Mandang & Yanagi, 2007)

4. METHODOLOGY

This study, as part of the water quality research carried out in the Mahakam Cluster of the East Kalimantan Project, builds on the results of the forward modelling by Mr. Syarif Budhiman (Budhiman, Salama, Vekerdy, & Verhoef, in preparation). A lookup table was built by forward modelling, and this was used for mapping water quality parameters with LANDSAT 7 ETM, MODIS AQUA and MODIS TERRA images. For validating the results, the MODIS map was compared to field data and then the LANDSAT 7 ETM and MODIS maps were compared with each other.

Below is flowchart of the study.

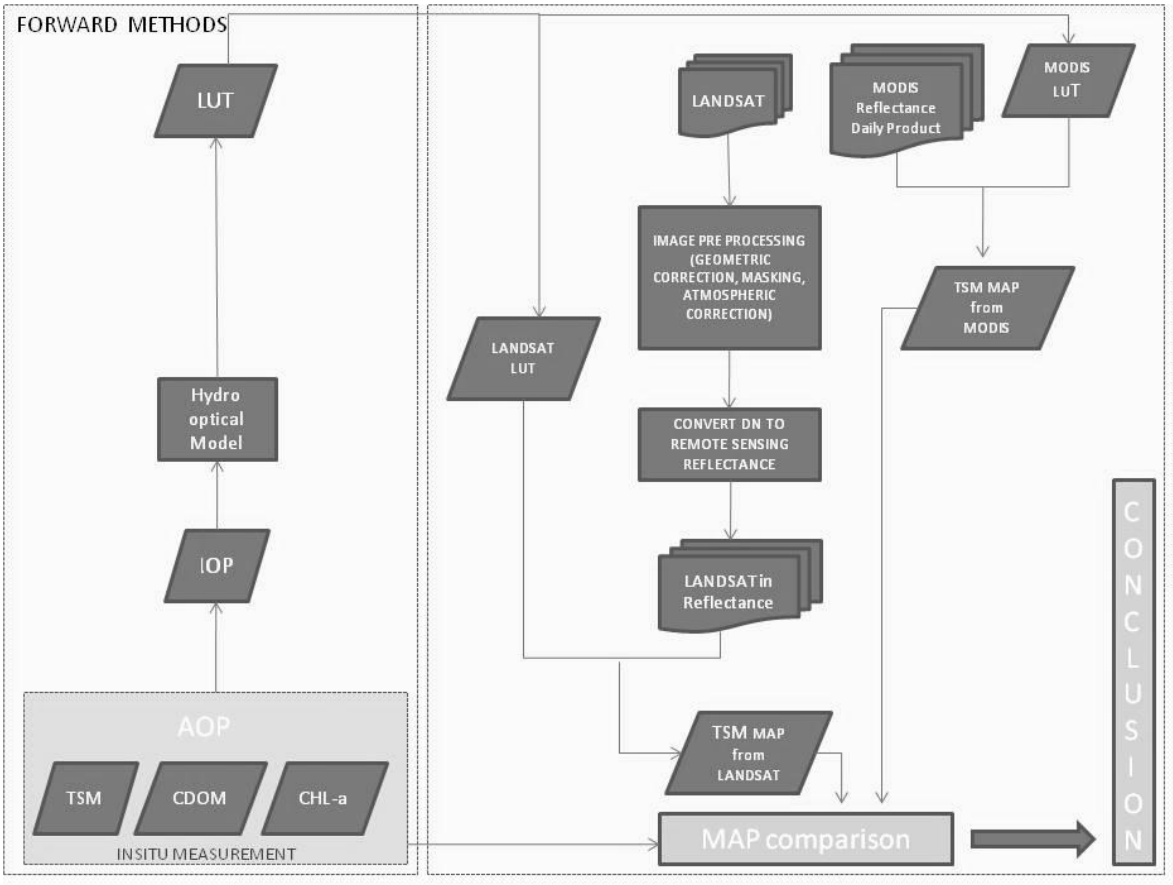

Figure 8. Research Flowchart

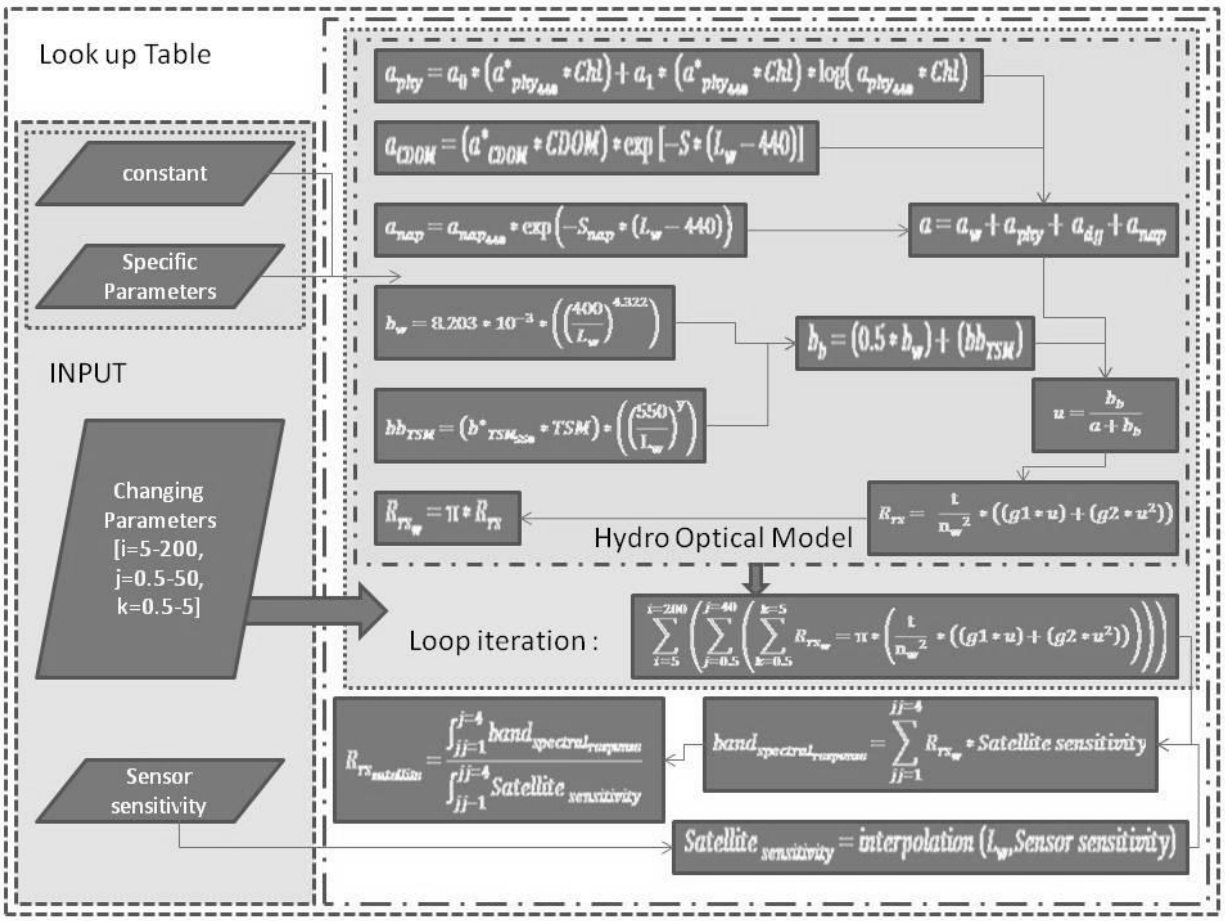

Figure 9. Look Up Table Flowchart

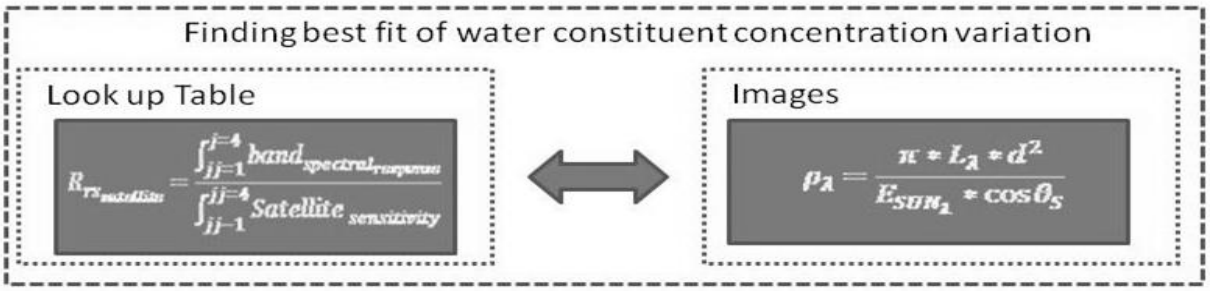

Figure 10. Look Up Table and Images Relationship

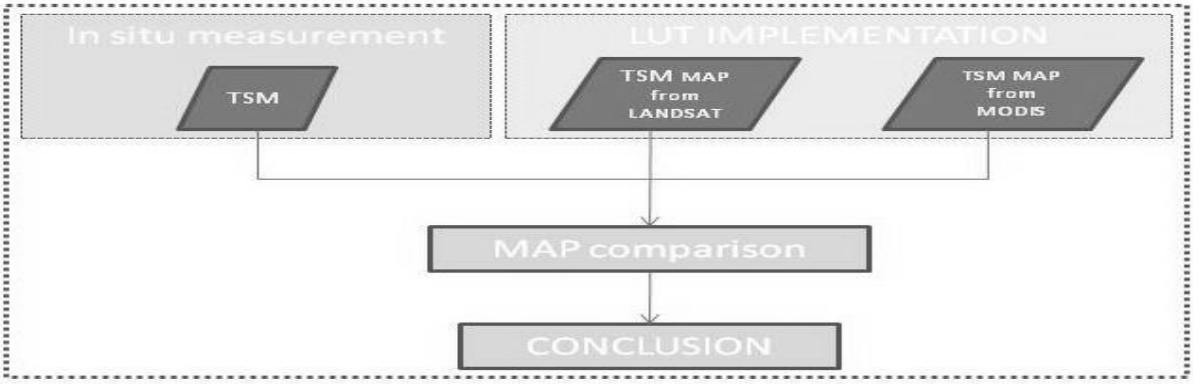

Figure 11. Research Validation

4.1. Data Sets

Data which is used in this study are remote sensing data sets, in-situ measurements data sets and coefficient data sets, and auxiliary data sets.

4.1.1. Remote Sensing Data Sets

In correspondence with the research objectives to map water quality parameters, LANDSAT 7 ETM, MOD09GA MODIS TERRA, and MYD09GA MODIS AQUA daily reflectance product is utilized in this study. Below in Figure 12 (A) and Figure 12 (B) are sample of the utilized remote sensing images.

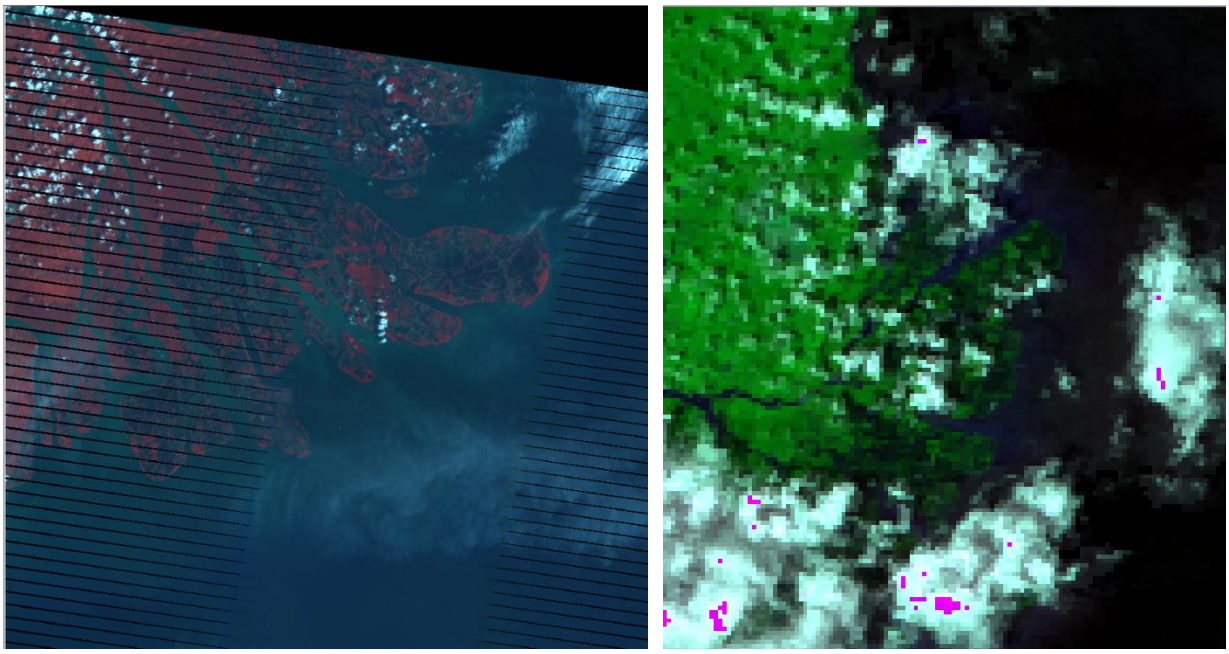

A B

Figure 12. (a) LANDSAT ETM; 1 Janury2007; (b) AQUA MODIS: 13 August 2008

LANDSAT 7 ETM and MODIS/AQUA surface reflectance daily product could be obtained from United State Geological Survey website at http://glovis.usgs.gov .

MOD09GA and MYD09GA are Level 2 surface reflectance products. It is created from the first seven bands of the full 36 band scene. It is a surface spectral reflectance estimation which would be measured at ground level without atmospheric effects. This data is provided in the Sinusoidal projection. It includes 1-kilometer observation geo-location statistics and 500-meter reflectance values. Each pixel corresponds to approximately a 10 degrees x 10 degrees (lat/long) area. MODIS AQUA and TERRA Surface Reflectance products are validated, meaning that product uncertainties are well defined over a range of representative conditions (NASA, 2010).

Remote sensing data sets acquisition information used in this study are listed in Table 1.

Table 1. LANDSAT 7 ETM, MYD09GA and MOD09GA acquisition data

Year	Satellite	Acquisition Date	Path/Row	Sun Zenith Angle [degree]	Sun Azimuth Angle [degree]
2007	LANDSAT 7 ETM	11 January 2007	116/60	36.9	125.9
	MYD09GA	11 January 2007	28/08	data sets	data sets
	MYD09GA	11 January 2007	28/09	data sets	data sets
	LANDSAT 7 ETM	1 April 2007	116/61	30.7	81.4
	LANDSAT 7 ETM	1 April 2007	116/60	31.2	79.1
	MYD09GA	1 April 2007	28/08	data sets	data sets
	MYD09GA	1 April 2007	28/09	data sets	data sets
2009	MYD09GA	05 August 2009	28/08	data sets	data sets
	MYD09GA	05 August 2009	28/09	data sets	data sets
	MYD09GA	06 August 2009	28/08	data sets	data sets
	MYD09GA	06 August 2009	28/09	data sets	data sets
	MOD09GA	06 August 2009	28/08	data sets	data sets
	MOD09GA	06 August 2009	28/09	data sets	data sets

4.1.2. In-situ Measurements

This study is using in-situ measurements collected by Syarif Budhiman (in-preparation) shown on Figure 13.

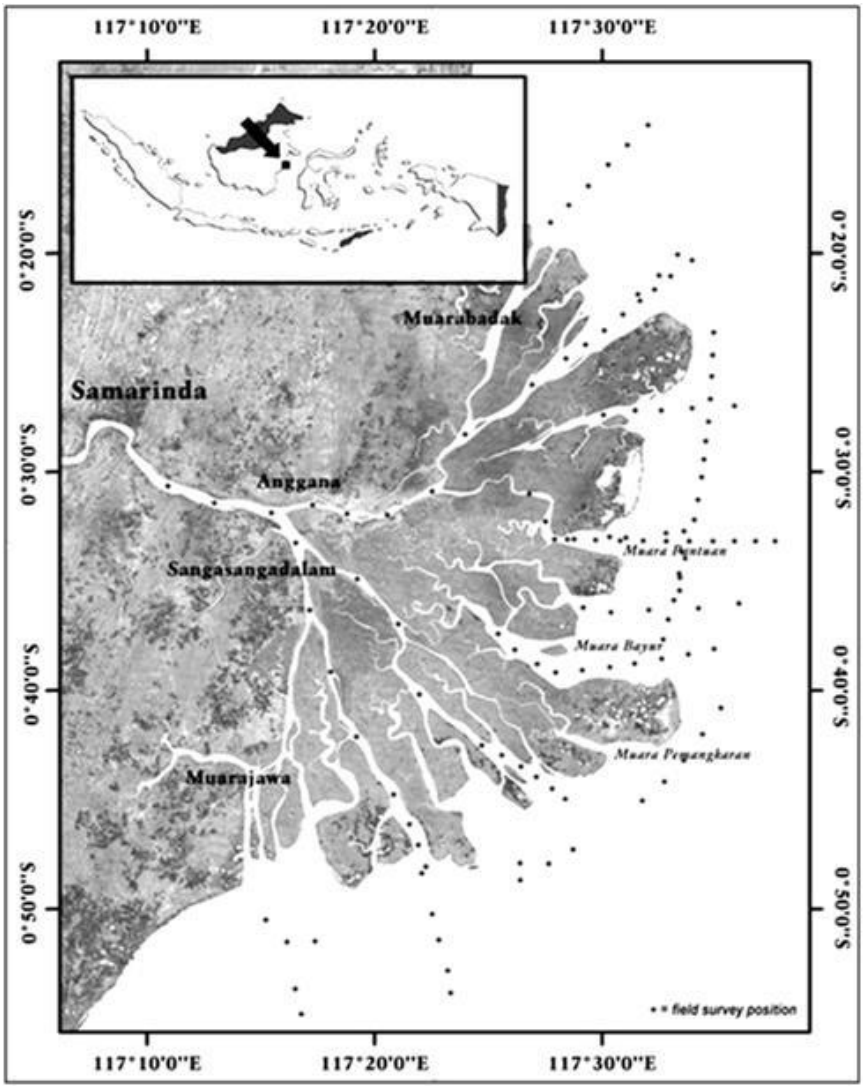

Figure 13. . Field measurement station

4.1.3. Coefficient Data Sets

Coefficient data sets used in this study are: a_w (water absorption) , a_0 and a_1 (empirical coefficients) (Lee, Carder, Mobley, Steward, & Patch, 1998)and gi (geometrical factor) (Maritorena, Siegel, & Peterson, 2002), y is TSM spectral shape parameter, S is CDOM spectral shape parameter, and S_{nap} detritus/non algae particle spectral shape parameters (Roesler, Perry, & Carder, 1989). Value of a_w , a_0 and a_1 can be found in the Appendix B. Value of gi, y, S, and S_{nap} can be found in Table 2.

Table 2. Constant Coefficient Parameters

g_1	=	0.0949	g_2	=	**0.0794**
y	=	0.579	S_{nap}	=	**0.011**
S	=	0.014			

Water constituent constant parameters shown below are used to build look up table 3. This water constituent is result of previous research carried in Mahakam Delta by Syarif Budhiman (in preparation).

Table 3. Mahakam Delta Input Parameters

$a^*_{phy_{440}}$	=	0.023[m^2g^{-1}]
$a^*_{dg_{440}}$	=	0.87 [m^2g^{-1}]
$a^*_{nap_{440}}$	=	1.51 [m^2g^{-1}]
$b^*_{TSM_{550}}$	=	0.008[m^2g^{-1}]

Where a^*_{phy} is phytoplankton specific absorption, a^*_{dg} is gelbstoff specific absorption, a^*_{nap} is detritus/non algae particle specific absorption, b^*_{SPM} is suspended sediment specific scattering.

4.1.4. Auxiliary Data Sets

The atmospheric correction input parameters (Table 4.) were obtained from several sources: The value of optical thickness were obtained from AERONET, NASA (2004), water vapour content were obtained from NASA(2004), the ozone content constant value was obtained from NASA (2009), and .air pressure was obtained from the weather underground website (WeatherUnderground, 1991).

Table 4. Auxiliary Data Sets as Input for Atmospheric Correction

YEAR	ACQUISITION DATE	AOD	Water Vapour	Ozone Content	Air Pressure
		0.05 - 0.8	0.0 - 6.0	0.0 - 0.7	
2007	11 January 2007	0.291	2.100	0.231	1009.000
	1 April 2007	0.396	4.700	0.250	1009.170

4.2. Software

Software used in this study are:

1. Integrated Land and Water Information System (ILWIS)
2. ERDAS
3. ENVI
4. MATLAB 2009a

4.3. Forward Method : Building Look Up Table

The objective of using forward modelling of this study is building look-up table for linking the AOP and water quality constituent concentrations. There were two look up tables build in this study, one for LANDSAT 7 ETM and one for MODIS.

4.3.1. The underlying theory

Look up table is developed from the in-situ measurements. Chlorophyll-a and SPM concentration measured from field campaigns (Budhiman, in-preparation) and the measured apparent optical properties

were linked as follows. The remote sensing reflectance (R_{rs}) is expressed using Garver-Siegel-Maritorena Model Version 1 (Maritorena, et al., 2002).

$$R_{rs} = \frac{\mathrm{t}}{\mathrm{n_w}^2} \sum_{i=1}^{2} gi * \left(\frac{b_b}{a + b_b}\right)^i \quad \text{Equation 4}$$

Where R_{rs} is Remote sensing reflectance; t is sea air transmission function (Maritorena, et al., 2002); $\mathrm{n_w}$ is water refraction index; gi is surface expansion coefficients due to internal refraction, reflection and sun zenith angle (Gordon et al., 1988); a is total absorption; and b_b is backscattering coefficient.

Total absorption is sum of all absorption. It could be parameterized below (D'sa & Miller, 2005):

$$a = a_w + a_{phy} + a_{dg} + a_{nap} \quad \text{Equation 5}$$

Where a_w is water absorption; a_{phy} is phytoplankton absorption; a_{dg} is colour detritus gelbstoff absorption; a_{nap} is detritus/non algae particle (nap) absorption.

The phytoplankton absorption a_{phy} mentioned in Equation 2 also can be parameterised below (Lee, et al., 1998):

$$a_{phy} = a_0 * \left(a^*{}_{phy_{440}} * Chl\right) + a_1 * \left(a^*{}_{phy_{440}} * Chl\right) * \log\left(a_{phy_{440}} * Chl\right) \quad \text{Equation 6}$$

Where $a^*{}_{phy}$ is phytoplankton specific absorption; and Chl is phytoplankton concentration [mg l^{-1}]; a_i is empirical coefficient of phytoplankton absorption (Lee, et al., 1998) ; and $a^*{}_{phy_{440}}$ is phytoplankton specific absorption at 440 nm wavelength.

Equation 4 above also could be parameterise below (Bricaud, Morel, & Prieur, 1981):

$$a_{CDOM} = (a^*{}_{CDOM} * CDOM) * \exp\left[-S * (L_w - 440)\right] \quad \text{Equation 7}$$

Where $a^*{}_{CDOM}$ is coloured detritus gelbstoff specific absorption; $CDOM_{440}$ is coloured detritus gelbstoff concentration at 440 nm wavelength [mg l^{-1}]; S is spectral decay constant for coloured detritus gelbstoff absorption; L_w is wavelength [nm], and $CDOM$ is coloured detritus gelbstoff concentration.

The detritus/non algae particle absorption parameters are below:

$$a_{nap} = a_{nap_{440}} * \exp\left(-S_{nap} * (L_w - 440)\right) \quad \text{Equation 8}$$

Where $a_{nap_{440}}$ is non algae particle specific absorption), S_{nap} is non algae particle spectral shape constant; and L_w is wavelength [nm].

The scattering parameter consists of water scattering parameter and total suspended matter backscattering parameters.

$$b_b = (0.5 * b_w) + (bb_{TSM})$$ Equation 9

And water backscattering could be parameterised below (Mobley, 2004):

$$b_w = 8.203 * 10^{-3} * \left(\left(\frac{400}{L_w}\right)^{4.322}\right)$$ Equation 10

While total suspended matter backscattering is parameterised below:

$$bb_{TSM} = \left(b^*{}_{TSM_{550}} * TSM\right) * \left(\left(\frac{550}{\mathrm{L_w}}\right)^{\mathrm{y}}\right)$$ Equation 11

Where b_w is water scattering; $b^*{}_{TSM_{550}}$ is total suspended sediment specific scattering; and TSM is suspended sediment concentration [mg l^{-1}]; $bb_{TSM}$is total suspended matter backscattering parameters; L_w is wavelength [nm]; and y is total suspended matter spectral shape parameter.

To simplify equation 4, absorption and backscattering equation could be identified as u

$$u = \frac{b_b}{a + b_b}$$ Equation 12

Equation 4 then could be written below:

$$R_{rs} = \frac{\mathrm{t}}{\mathrm{n_w}^2} * \left((g1 * u) + (g2 * u^2)\right)$$ Equation 13

Remote sensing reflectance should be converted into water remote sensing reflectance factor by multiply it with π (Gordon, et al., 1988; Maritorena, et al., 2002). In this stage, unit of remote sensing reflectance value in look up table would be the same with water remote sensing reflectance from image.

$$R_{rs_w} = \pi * R_{rs}$$ Equation 14

Equation 14 could be written as below:

$$R_{rs_w} = \pi * \left(\frac{\mathrm{t}}{\mathrm{n_w}^2} * \left((g1 * u) + (g2 * u^2)\right)\right)$$ Equation 15

4.3.2. Iteration

Look up table is built by nested looping as follows:

$$\sum_{i=5}^{i=200} \sum_{j=0.5}^{j=40} \sum_{k=0.5}^{k=5} R_{rs_w} = \pi * \left(\frac{\mathrm{t}}{\mathrm{n_w}^2} * \left((g1 * u) + (g2 * u^2)\right)\right)$$ Equation 16

Where i controls TSM concentration with $\Delta TSM = 2.5\, mg.l^{-1}$, j controls Chl concentration with $\Delta Chl = 0.5\, mg.l^{-1}$, and k controls $CDOM$ concentration with $\Delta CDOM = 0.5\, mg.l^{-1}$. R_{rs_w} is water remote sensing reflectance, t is sea water air transmission function, $\mathrm{n_w}$ is water refraction index, *gi* is surface expansion coefficients due to internal refraction, reflection and sun zenith angle, u = equation 12.

Result of look up table is table of R_{rs} value with input variations.

4.3.3. Spectrum

Spectrum resolution applied in this look up table is 10 nm.

4.3.4. Sensor Sensitivity

Both remote sensing data used in this study has different spectral sensitivity. Look up table has to considering this spectral sensitivity. Wavelengths and sensor sensitivity were interpolated linearly to obtain each satellite data sensitivity. LANDSAT 7 ETM sensor's sensitivity source was taken from LANDSAT's handbook (NASA, 2009) whilst MODIS sensor sensitivity was taken from The U.S. Government Public Information Exchange Resource (2002). Value of sensor sensitivities could be found at appendix section.

$$Satellite\ _{sensitivity} = interpolation\ (L_w, Sensor\ sensitivity) \qquad \text{Equation 17}$$

4.3.5. Band Weight

Water remote sensing reflectance from equation 16 needs to be multiplied by satellite sensitivity (equation 16) to obtained band spectral response.

$$SR_n = \sum_{\lambda_{min}(n)}^{\lambda_{max}(n)} R_{rs_w}(\lambda) * S(\lambda) \qquad n = 1 \ldots m \qquad \text{Equation 18}$$

Where SR_n is the spectral response of band n, R_{rs} is the remote sensing reflectance; w stands for water, n is the band number, $S(\lambda)$ is the sensitivity of the sensor at λ wavelength, and m is the number of bands. At this stage, a look up table was calculated using the inherent optical properties defined by Budhiman (2010), and the spectral sensitivity of each satellite band, that was ready to be used to retrieve water constituent concentrations from the remote sensing images.

4.4. Inverse Methods

4.4.1. LANDSAT Image Pre-Processing

4.4.1.1. Radiometric Correction: DN to Radiance

In order to interpret information, the pixel values (in dimensionless digital numbers, DN's) were converted to units of absolute radiance. Equations 20 and 21 were used to convert DN's into radiance units (NASA, 2009)

$$L_\lambda = Grescale * Q_{CAL} + Brescale \quad \text{Equation 19}$$

Equation 20 above also could be express with equation 21 below:

$$L_\lambda = \left(\frac{L_{MAX_\lambda} - L_{MIN_\lambda}}{Q_{CALMAX_\lambda} - Q_{CALMIN_\lambda}}\right) * \left(Q_{CAL} - Q_{CALMIN_\lambda}\right) + L_{MIN_\lambda} \quad \text{Equation 20}$$

Where L_λ is spectral radiance at sensor aperture [W m^{-2} sr^{-1} μm^{-1}]; *Grescale* is the gain [W. m^{-2}. sr^{-1}. μm^{-1}. DN^{-1}]; *Brescale* is the offset; Q_{CAL} the pixel value [DN]; Q_{CALMAX_λ} the maximum pixel value [DN]; Q_{CALMIN_λ} is the minimum pixel value [DN]; L_{max_λ} is maximum spectral radiance which is scaled to Q_{CALMAX_λ} [W. m^{-2} . sr^{-1} . μm^{-1}]; L_{min_λ} is minimum spectral radiance which is scaled to Q_{CALMIN_λ} [W. m^{-2} . sr^{-1}. μm^{-1}].

4.4.1.2. Radiometric Correction: Radiance to Reflectance

Solar irradiance normalization by converting spectral radiance into planetary reflectance is needed to reduce the in-between scene variability of LANDSAT 7 ETM image. Formula to convert radiance as follow (NASA, 2008):

$$\rho_\lambda = \frac{\pi * L_\lambda * d^2}{E_{SUN_\lambda} * \cos\theta_S} \quad \text{Equation 21}$$

Where ρ_λ is unit-less planetary reflectance; L_λ is spectral radiance; d is earth-sun distance [astronomical units]; E_{sun_λ} is mean solar exoatmospheric irradiance [Wm^{-2} μm^{-1}]; θ_s is solar zenith angle [degree].

Table 5 is the Solar exoatmospheric irradiance in LANDSAT (NASA, 2009):

Table 5. LANDSAT Solar Exoatmospheric Irradiance

Bands	**Wm^{-2} μm^{-1}**
1	1997
2	1812
3	1533
4	1039

4.4.1.3. Atmospheric Correction

Atmospheric correction is an image processing step where the atmosphere influence is eliminated (Wang & DeLiberty, 2005) to retrieve water leaving reflectance. This correction is an important step to obtain real important information from water body which should be done before interpretations of water signal could be performed (IOCCG, 1998). From several methods, SMAC (Rahman & Dedieu, 1994) is chosen to be used to remove the atmospheric effect on image.

SMAC was build from 5S model (Rahman & Dedieu, 1994). Input parameters are important in this stage to retrieve correct water leaving reflectance (Vermote et al., 2005). Input data used to perform atmospheric correction are listed in Table 5.

The value of optical thickness were obtained from AERONET, NASA (2004). Another important input is water vapour content which were obtained from NASA(2004). The ozone content constant value was obtained from NASA (2009). Total ozone content was measured by the Ozone Monitoring Instrument (OMI) carried by the Aura spacecraft.

4.4.2. MODIS Image Pre-Processing

MODIS data used in this study are MODIS AQUA and TERRA daily reflectance product. Thus, no other actions were needed to obtain reflectance data than rescaling the cell values by dividing them by 10,000. These data then were stored with a floating point data type and converted from Sinusoidal to UTM projection.

4.4.3. Land and Clouds Masking

Land and clouds masking was done to limit the image on water only and also to reduce the routine load during look up table implementation. This masking was using ratio between red band and near infra red band (Ouaidrari & Vermote, 1999). Land boundary value applied on image was 1.1, thus all value equal and above 1.1 was assigned as land. Clouds boundary was taken from lowest clouds value at near infra red band.

4.4.4. Subset

Subset was created to focus the study area and also to reduce the processing load on look up table implementation.

4.5. Apply Look up Table

4.5.1. Reading Image

All images in reflectance form were applied to look up table to find the best water constituent concentration variation fit. After stacking all bands into one raster map, it was saved in ENVI format file. This ENVI format file was processed in MATLAB to obtain the map.

4.5.2. Finding Minimum Value and its Position

When look up table is implemented to an image, match water constituent concentration combinations to a pixel of 4 bands consist in the image would be resulted. From these variant water constituents' concentration combination, the most matching water constituent concentration combination is assigned as the end result. The minimum value of sum error from each water constituent concentration combination at each band would be the indicator of the best match among all variant possibilities.

5. RESULT AND DISCUSSION

This study aims to map total suspended matter using low temporal-high spatial resolution and high temporal-low spatial resolution satellite data with look up table inversion (developed by Budhiman 2010). There were two major steps of this study. The first is building look up table and the second is look up table implementation on remote sensing imagery of the Mahakam delta, Indonesia.

5.1. Water Leaving Reflectance

Satellite imagery used in the look up table inversion were in water leaving reflectance values of the visible bands. This is because water leaving reflectance defines the water colour that contains information on the inherent optical properties and water constituents (D'sa & Miller, 2005; Salama & F, 2009).

There are two steps of the retrieval water of colour information from remote sensing imagery. The first is retrieving water leaving reflectance as product of atmospheric correction, and secondly retrieving water constituent concentration which determined from water leaving reflectance (Liang, Fang, & Chen, 2001; Yu-Hwan Ahn, 2004). Atmospheric correction is a requirement step before any water colour signal examination can be made (IOCCG, 1998). This is due to atmosphere effect which is reducing radiometric accuracy of images *(*Norjamaki *& Tokola, 2007).*

5.1.1. Atmospheric Correction

LANDSAT 7 ETM water leaving reflectance used in this study was derived by removing atmospheric effect using the Simplified Method for Atmospheric Corrections (SMAC).

Prior in selecting SMAC as atmospheric correction method, the Second Simulation of a Satellite Signal in the Solar Spectrum (6S) was also applied to the same images. However the atmosphere effect model result from 6S was giving negative water leaving reflectances for some pixels. This most probably happened due to the poor quality of the available model parameters.

Finding an accurate input parameter to remove the atmospheric effect in this study was a big challenge. This is because there were no actual weather parameters on study area which coincide with image acquisition dates. All input parameter used in the atmospheric correction method was derived from auxiliary sources which has the closest position to the study area. Sources of input parameter were mentioned in section 4.4.1.3 Atmospheric Correction.

Atmospheric correction was not applied to MODIS AQUA daily reflectance and MODIS TERRA daily reflectance used in this study because both data type is second level data which are atmospherically corrected (USGS, 2010).

Another challenge in retrieving water leaving reflectance is cloud masking and haze. Study area is located in tropical humid area, which always covered by clouds.

5.1.2. LANDSAT 7 ETM Water Leaving Reflectance Images

Land and clouds were masked from remote sensing imagery in order to concentrate on water area only. Figure 14 shows water leaving reflectance from LANDSAT 7 ETM on 11 January 2007, while Figure 15 shows water leaving reflectance from LANDSAT 7 ETM on 1 April 2007.

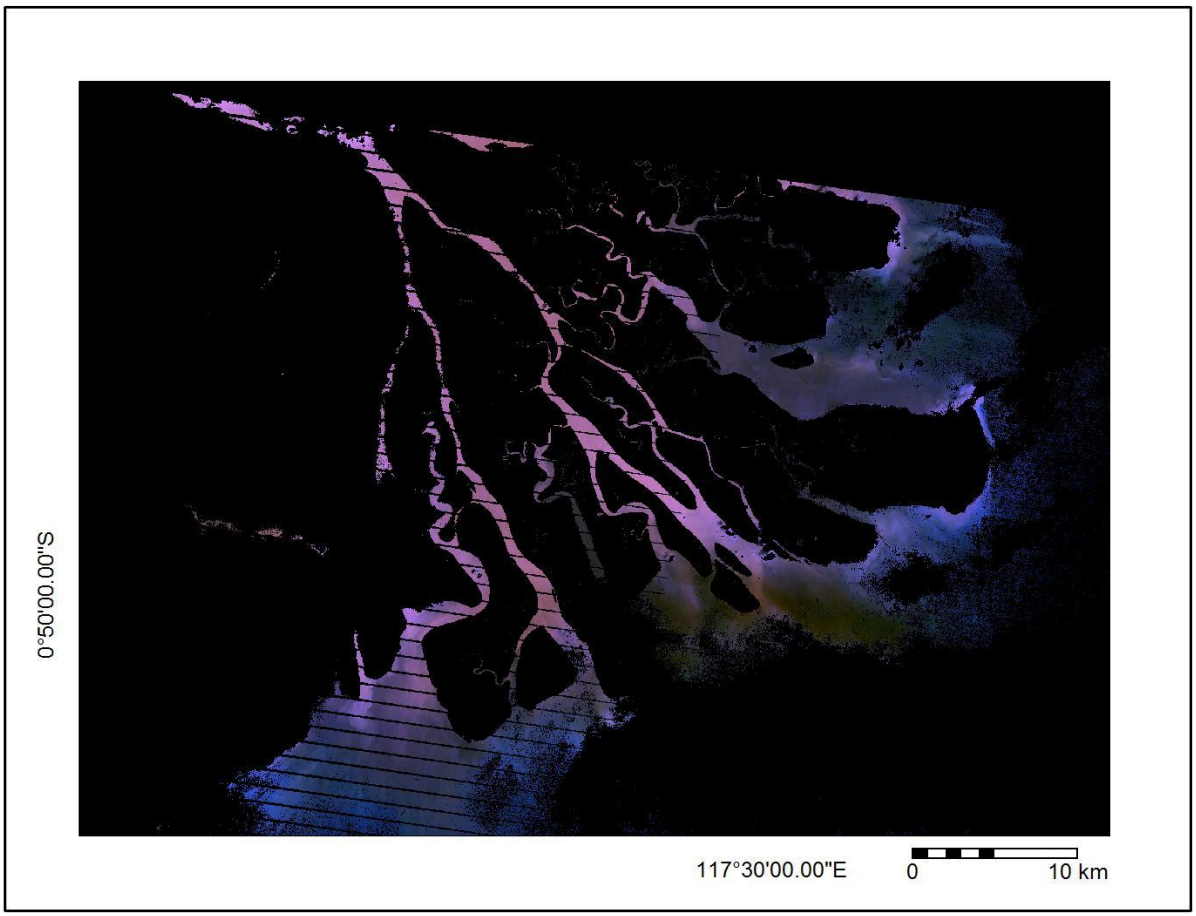

Figure 14. LANDSAT 7 ETM taken on 11 January 2007 after atmospheric correction with true colour 3-2-1 Band Composite.

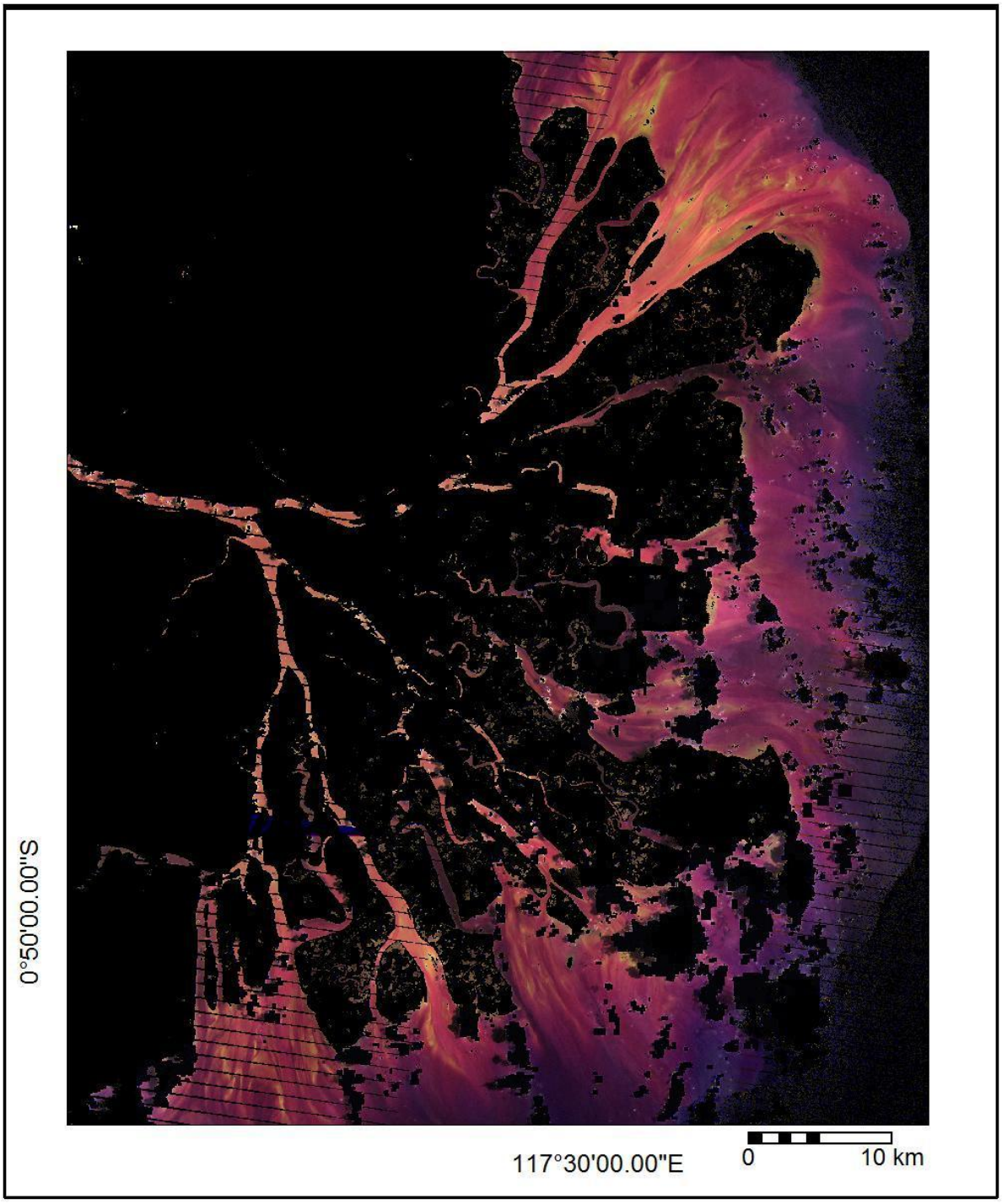

Figure 15. LANDSAT 7 ETM taken on 1 April 2007 after atmospheric correction with true colour 3-2-1 Band Composite.

5.2. Look Up Table

Two look up tables were build to invert remote sensing images used in this study. Both remote sensing image types have different spectral sensitivity range. Figure 16 shows LANDSAT 7 ETM and MODIS daily reflectance wavelength sensitivity range. Visible wavelength are used in water quality studies due to

their water column penetration (Robinson, 1994). Band 1, band 2, and band 3 of LANDSAT 7 ETM and band 1, band 3, and band 4 of MODIS daily reflectance are also in visible wavelength range.

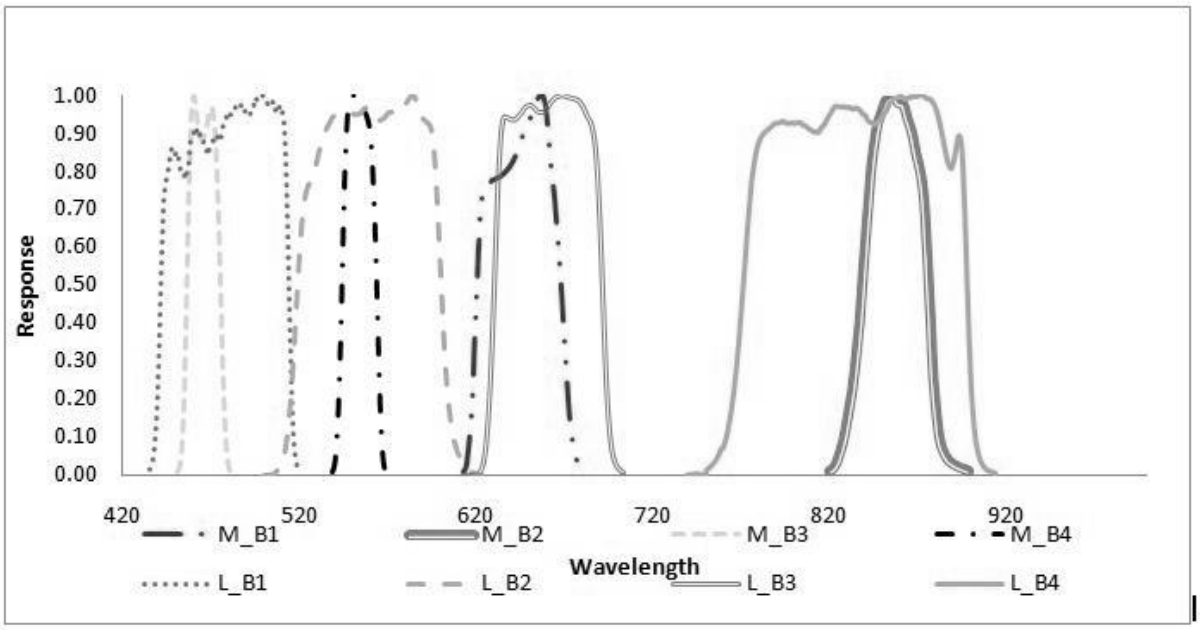

Figure 16. Band Response Sensitivity of LANDSAT 7 (L_B1 – L_B4) (NASA, 2009) and MODIS (M_B1 – M_B4) Daily reflectance (U.S. Government Public Information Exchange Resource, 2002)

Water Colour Coefficient data sets used in this study was taken from several previous researches such as sea air transmission function (*t*) (Maritorena, et al., 2002), water index refraction (n_w), surface expansion coefficients due to internal refraction, reflection and sun zenith angle (*gi*) (Gordon, et al., 1988), water absorption (a_w) (Pope & Fry, 1997), empirical coefficient of phytoplankton absorption (a_i) (Lee, et al., 1998).

Mahakam delta specific coefficients were taken from previous research conducted by Syarif Budhiman (in preparation). Those specific coefficients are $a^*_{phy_{440}}$, $a^*_{dg_{440}}$, $b^*_{SPM_{550}}$.

5.2.1. Forward Method: Building Look up Table

Gordon model was used to calculate inherent optical properties while forward model was used in building look up table. Equation 24 is showing how the iteration should be done.

Mechanism of look up table iteration (Equation 16) is shown in Table 6. Iteration was started at $i = 5\ mg.l^{-1}$, $j = 0.5\ mg.l^{-1}$ and applied to a whole k range. When the first iteration finish, it would continue to second iteration at $i = 5\ mg.l^{-1}$, $i = 1\ mg.l^{-1}$ and applied to a whole k range. Again, when the second iteration finish, iteration would continue until $i = 200\ mg.l^{-1}$, $j = 40\ mg.l^{-1}$ and applied to a whole k range.

Table 6. Variations of TSM, Chl, $CDOM$ combination in the numerical computation

$TSM(\Delta TSM = 2.5\, mg.l^{-1})$	$Chl(\Delta Chl = 0.5\, mg.l^{-1})$	$CDOM(\Delta CDOM = 0.5\, mg.l^{-1})$
5	0.5	0.5
5	0.5	1.0
5	0.5	1.5
5	0.5	2.0
...	...	...
...	0.5	5
...	1.0	0.5
...	1.0	1.0
...	...	1.5
...	...	2.0
...	...	...
...	1.0	5
...	1.5	0.5

Considering that sum of $i = 80$, sum of $j = 81$, sum of $k = 11$ then there would be 35,640 water constituent concentration combination possibilities for each band.

5.2.2. Look up Table Validation

In order to validate this look up table, remote sensing reflectance derived from look up table was compare to remote sensing reflectance derived from Water Colour Simulation tools (WASI). WASI integrates forward and inverse model for eight aquatic optical in situ measurements, among others absorption, attenuation, specular reflectance, irradiance reflectance, remote sensing reflectance, bottom reflectance, down welling irradiance and upwelling radiance. It can be used generate, analyse and visualise water spectra (Gege, 2004).

Figure 17 (A) shows Remote sensing reflectance derived from look up table and Figure 17 (B) shows Remote sensing reflectance from WASI. Both were simulating Remote sensing reflectance at $i = 0, 50, 100, 150, 200, 250, 300, 350, 400, 450, and\ 500\, mg.l^{-1}$, $j = 1\, mg.l^{-1}$ and $k = 0.5\, mg.l^{-1}$ range. The two remote sensing reflectance graphs are similar, therefore the forward modelling method can be considered correct and the look up table is assumed to derive a correct concentration.

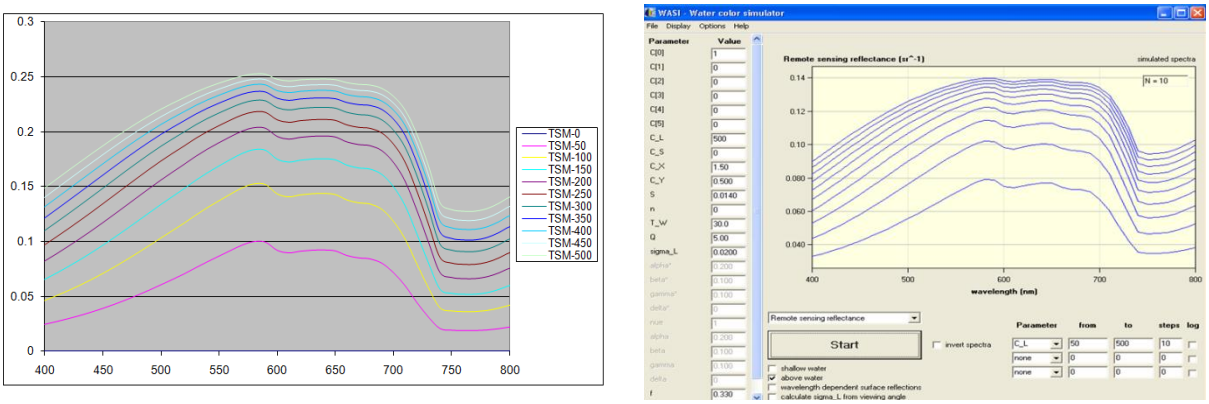

A B

Figure 17. (A) Remote sensing reflectance derived from look up table and (B) remote sensing derived from WAter colour Simulation.

5.3. Look up Table implementation

Look up tables were implemented to water leaving reflectance on remote sensing imagery. The most matching water constituent concentration combinations of each band were assigned as end result of the look up tables. The four-band combination of the pixel is compared to 35,640 four-band combinations stored in the LUT. The minimum sum error of matched water constituent combination for all band in the pixel were assigned as the correct water constituent concentration.

To save computation time, subsets were created from the LANDSAT 7 ETM water reflectance images.

To save computation time, subsets were created from the LANDSAT 7 ETM water reflectance images. However, the look up table implementation performance depends on the computer performance too. Even though five computers were used to implement all small pieces of image, still, some of images needed days to complete the implementation.

The look up table implementation on MODIS imagery did not require long time as LANDSAT 7 ETM imagery because the pixel number is much less than LANDSAT 7 ETM.

5.3.1. Best fit Images Value from Look up table

TSM map was derived by look up table implementation. Land and clouds were masked from remote sensing imagery in order to concentrate on water area only. In the output, the land is marked with the coastline and TSM concentration map is present in colour range (Figures 18 – 21).

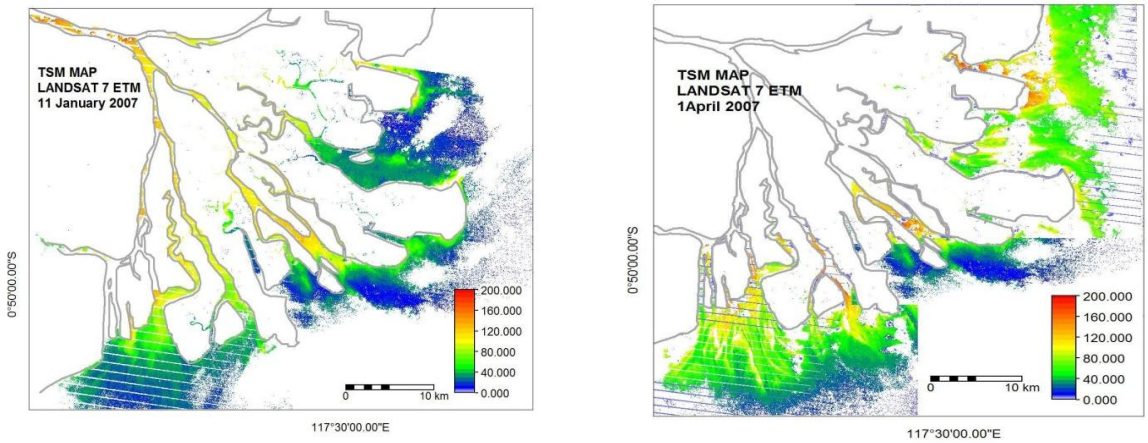

A B

Figure 18. (A) TSM MAP derived from LANDSAT 7 ETM taken on 11 January 2007 at 10.00-10.15AM; (B) TSM MAP derived from LANDSAT 7 ETM taken on 1 April 2007 at 10.00-10.15 AM

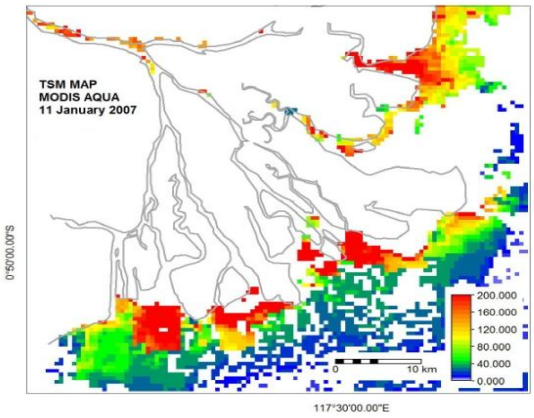

Figure 199. TSM MAP derived from MODIS AQUA Daily Reflectance taken on 11 January 2007 at 01:30PM

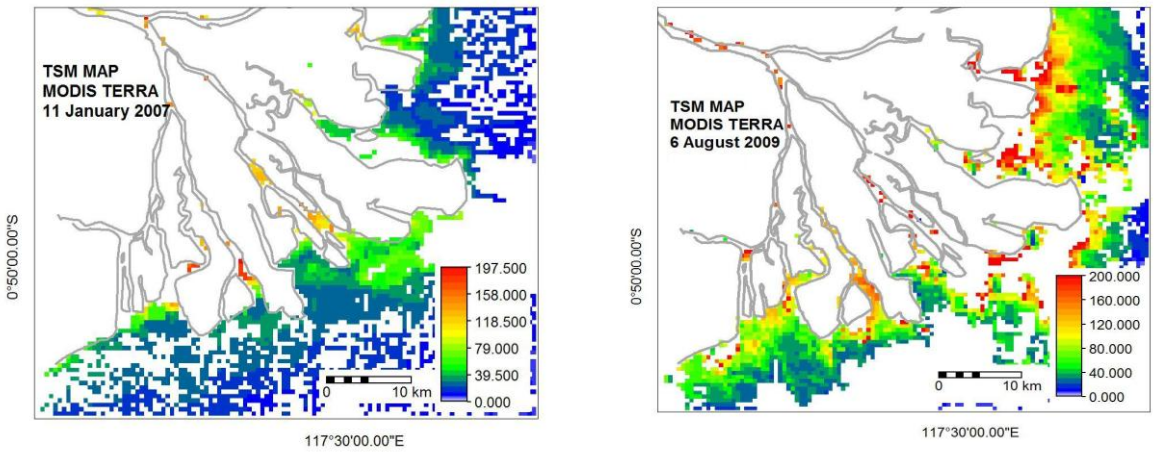

A B

Figure 200. (A) TSM MAP derived from MODIS TERRA Daily Reflectance taken on 11 January 2007 at 10:30AM; (B) TSM MAP derived from MODIS TERRA Daily Reflectance taken on 6 August 2009 at 01:30PM

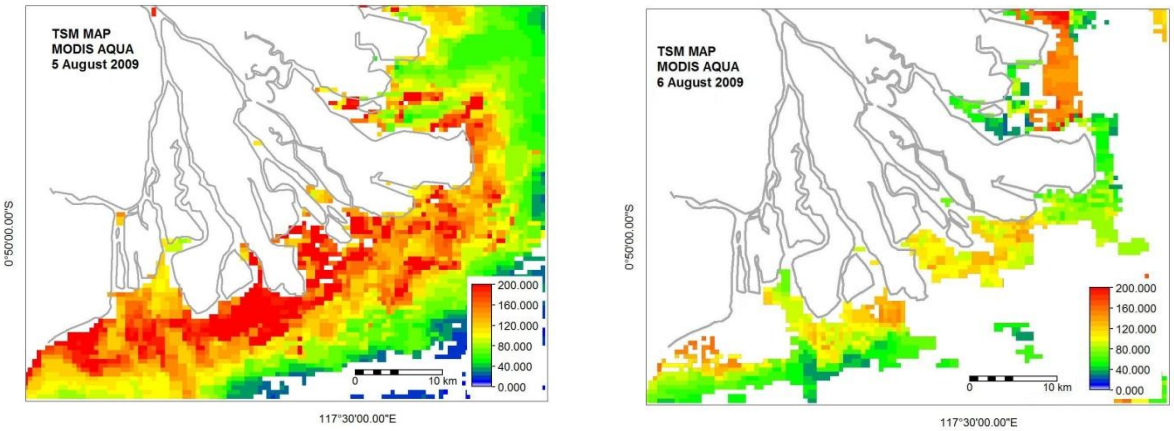

A B

Figure 211. (A) TSM MAP derived from MODIS AQUA Daily Reflectance taken on 5 August 2009 at 01:30PM; (B) TSM MAP derived from MODIS AQUA Daily Reflectance taken on 6 August 2009 at 01:30PM

Comparison of maps derived from remote sensing imagery taken around 10:00-10:30 AM and at 01:30 PM, reveals of different patterns. Figure 18 (A), Figure 18 (B), and Figure 20 (A) shows that high TSM concentrations are located in the distributaries (fluvial) channels and the channel mouths.

Massive oversaturated TSM concentration area (red colour) shown from Figure 21 (A) is assumed to be haze which was adding to the reflectance, but was not removed by atmospheric correction (most probably due to insufficient parameterization). Thus, this high reflectance was assigned as high concentration of TSM. Furthermore, in some pixels the actual concentration may be beyond the maximum which was assigned during look up table development (TSM concentration is ranging between 5-200 mgl^{-1}).

5.4. Validation of the TSM maps with in situ data

Map validation by direct comparison with in situ measurement is necessary to be done (Santoleri, Nardelli, & banzon, 2002). There are 8 in situ measurements measurement points where the sampling coincided with MODIS AQUA and MODIS TERRA image acquisition on 6 August 2009.

Comparing the in situ measurements to the TSM maps derived from MODIS TERRA and MODIS AQUA daily reflectance, it is found that not all of the points have corresponding TSM concentration on the map (See Figure 22 (A) and Figure 22 (B)). On TSM map derived from MODIS TERRA daily reflectance (Figure 22 (A)), the water area (non masked area) is larger compared to the TSM map which was derived from MODIS AQUA daily reflectance (Figure 22 (B)). This related to their time acquisition. MODIS TERRA was taken in the morning (10:30 AM), when normally clouds still have not formed yet.

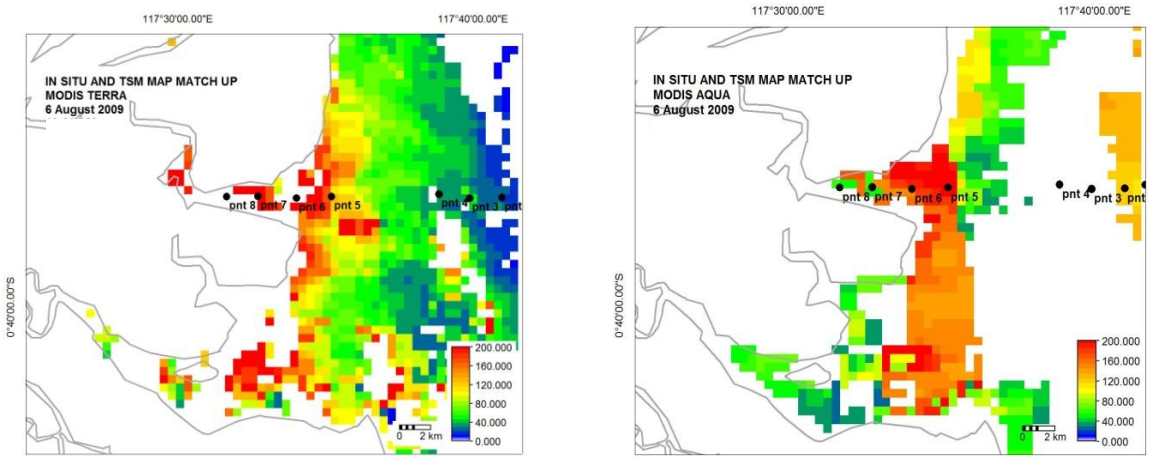

A B

Figure 222. (A) In situ measurement match up with TSM map derived from MODIS TERRA daily reflectance on 6 August 2009 at 10:30 AM; (B) In situ measurement match up with TSM map derived from MODIS AQUA daily reflectance on 6 August 2009 at 01:30 PM

The comparison between in situ TSM concentration and TSM map derived from MODIS TERRA daily reflectance on 6 August 2009 (TSM_MT06) and TSM map derived from MODIS AQUA daily reflectance on 6 August 2009 (TSM_M06) can be seen on Table 7.

Table 7. In situ and TSM map comparison

Point	TSM in situ (mg.l^{-1})	TSM_MT06 (mg.l^{-1})	TSM_M06 (mg.l^{-1})
1	22		
2	26	25	
3	18	40	
4	36	31	
5	172	150	200
6	126		145
7	70		55
8	16		60

The plot of TSM concentration from Table 8 can be seen in Figure 23. It shows a good fit between the in situ TSM concentrations and TSM concentrations derived from MODIS AQUA daily reflectance and MODIS TERRA daily reflectance. The statistical analysis was made using RMSE and type II regression can be seen in Table 8.

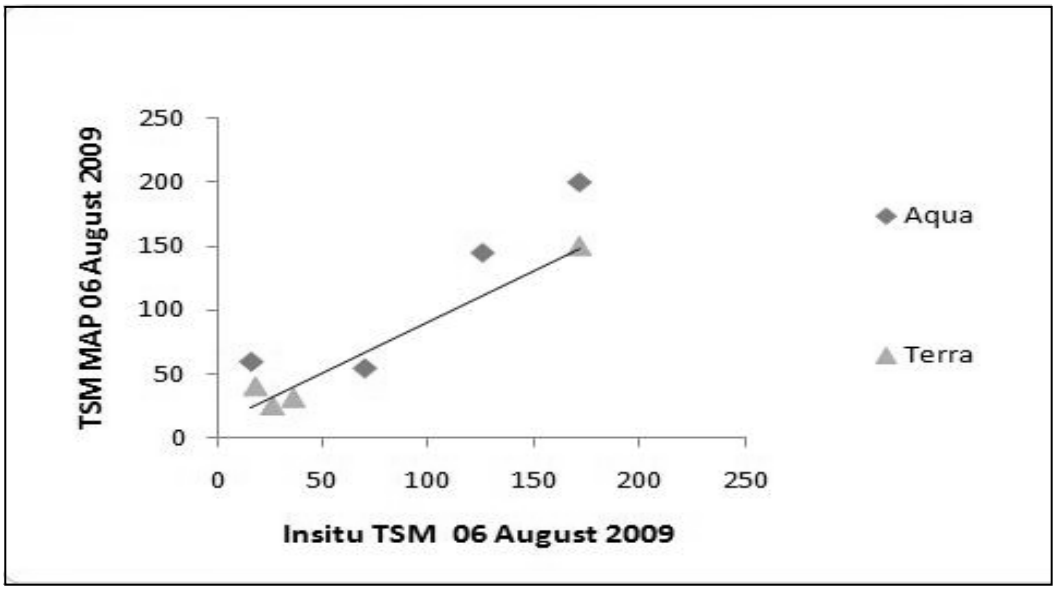

Figure 23. Comparison between in situ TSM Concentration and TSM Concentration derived from MODIS AQUA daily reflectance and MODIS TERRA daily reflectance

Considering statistical analysis result in Table 8, it can be assumed that look up table can be used to derive TSM concentration. From data plotting on Figure 23, it can be seen that between TSM concentration derived from MODIS TERRA and MODIS AQUA daily reflectance are relatively close each other. This is can be concluded that both, MODIS TERRA and MODIS AQUA daily reflectance can be used to derived TSM concentration.

Table 8. RMSE and type II regression parameter between in situ TSM Concentration and TSM Concentration derived from MODIS AQUA daily reflectance and MODIS TERRA daily reflectance

	No Samples	Slope	Intercept	R^2	RMSE
TSM_M06	4	0.968586	22.01571	0.8746828	0.1475
TSM_MT06	4	0.79905	11.15984	0.9679127	0.0895

However, this assumption is not secure since it was only test 8 point measurement in total. It should be noted also that the values which were compared have a good distribution.

5.5. Comparison of TSM concentrations derived from MODIS TERRA and LANDSAT 7 ETM

Unfortunately there was no in situ measurement coinciding with LANDSAT image acquisition. Assuming that TSM concentrations derived from MODIS daily reflectance is match with in situ measurement, MODIS daily reflectance could be act as a reference in comparing with TSM concentration derived from LANDSAT 7 ETM.

Two TSM maps from MODIS TERRA daily reflectance and LANDSAT 7 ETM dated 11 January 2007 were compared. These images were chosen because both were taken practically in the same time. From Figure 24, it is shown that both TSM maps show similar pattern. LANDSAT 7 ETM which has smaller pixel size than MODIS pixel size gives a more detail image than MODIS.

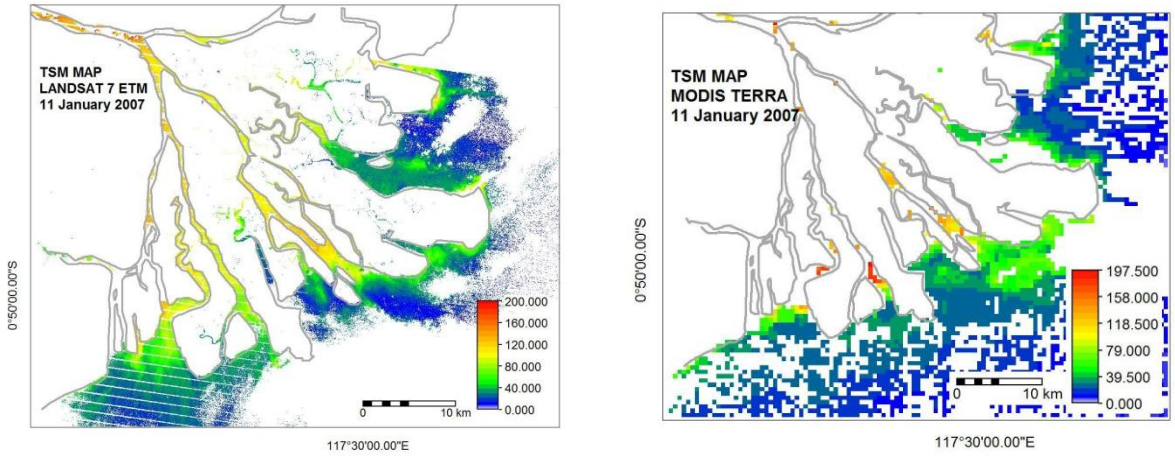

A B

Figure 244. (A) TSM map derived from LANDSAT 7 ETM on 11 January 2007 at 10:00-10:15AM; (B) TSM map derived from MODIS TERRA daily reflectance on 11 January 2007 at 10:30AM.

To make an accurate comparison, overlaying areas were chosen. The area should be free from adjacency effect, clouds, land area and SLC off effect for LANDSAT 7 ETM image. Masking was done to remove the unwanted area.

Since LANDSAT 7 ETM pixel size is smaller than MODIS pixel size, TSM map spatial resolution derived from LANDSAT 7 ETM was upscaled to MODIS spatial resolution. First a 15 x 15 average filter was applied to TSM map derived from LANDSAT 7 ETM. This is done in order to make 15 x 15 pixel average area which then would be used to resample it to the TSM map which was derived from MODIS TERRA (Figure 25 (A)).

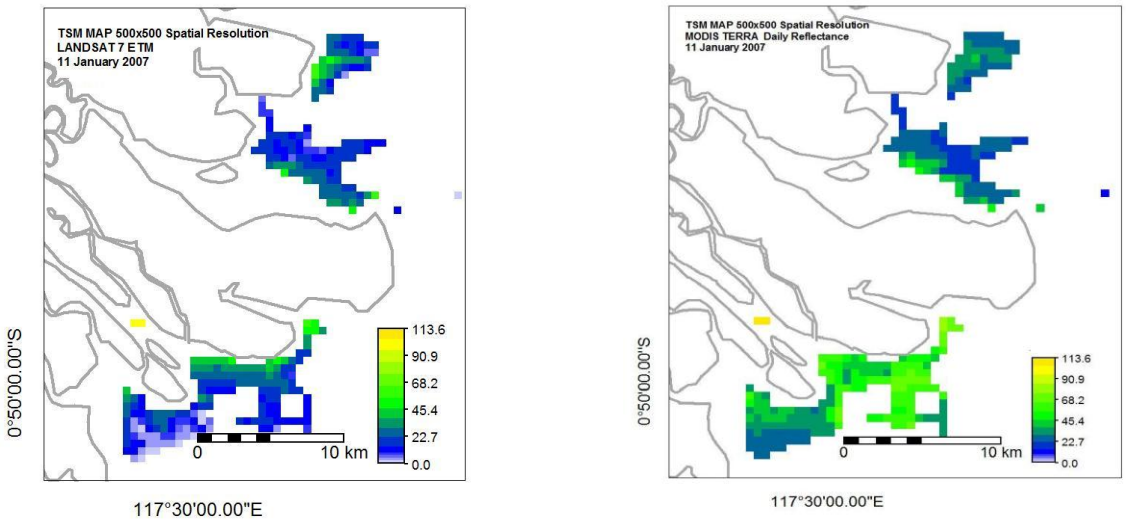

A B

Figure 255. (A) TSM map derived from LANDSAT 7 ETM 500x500 m Spatial Resolution; (B) TSM map derived from MODIS TERRA daily reflectance

The selected comparison area from both TSM maps has 319 pixels for comparison. Scatter plot of all pixels can be seen in Figure 26. It shows that the TSM concentrations derived from LANDSAT 7 ETM underestimate the ones derived from MODIS TERRA. From statistical analysis in Table 9, it can be seen that the correlation between the data is weak. This is probably because pixels in the comparison area do not have a high TSM concentration range. Another assumption of reason behind this discrepancy is maybe this is due to the value difference between both images (Figure 25 (A) and Figure 25 (B)).

Table 9. RMSE and type II regression parameter between TSM map derived from MODIS TERRA daily reflectance and TSM map derived from LANDSAT 7 ETM

N	slope	intercept	R^2	RMSE
319	0.393559	5.743431	0.210964	0.468174

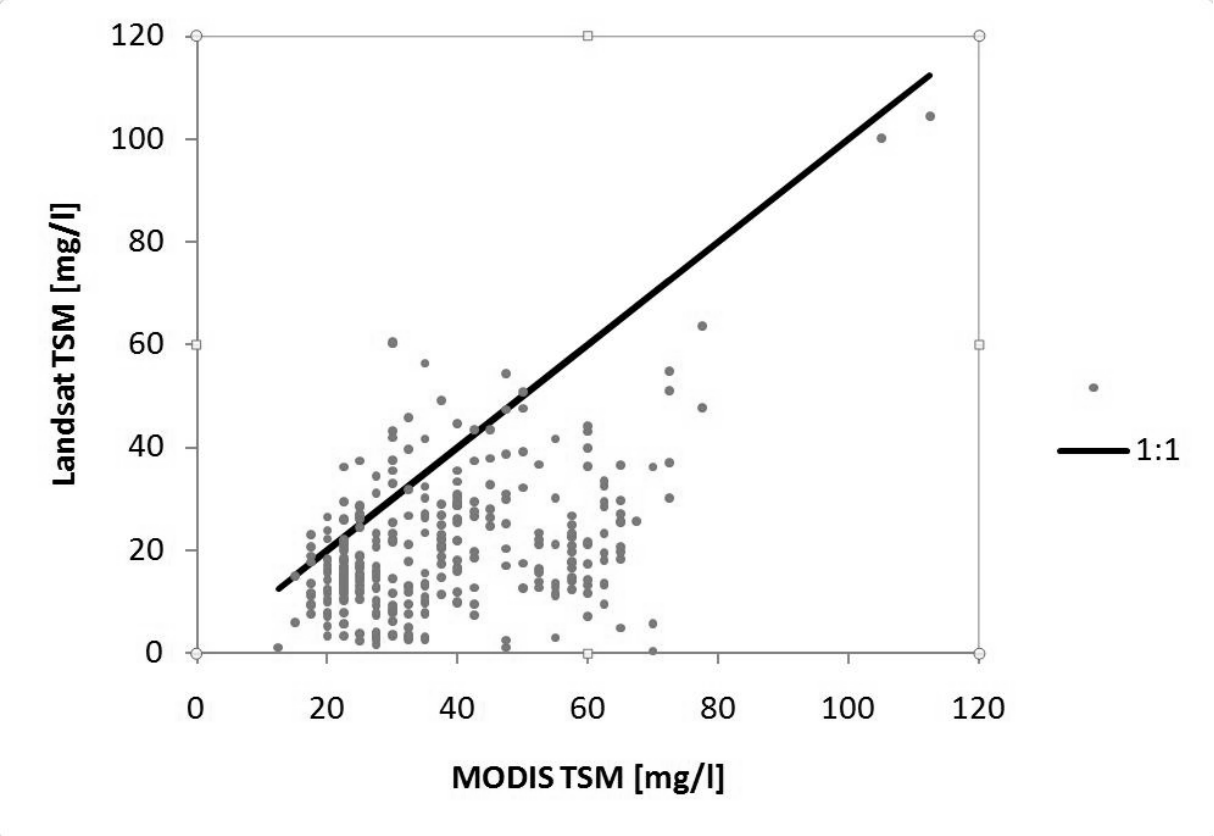

Figure 266. Comparison between TSM map derived from MODIS TERRA daily reflectance and LANDSAT 7 ETM

6. CONCLUSIONS AND RECOMMENDATIONS

6.1. CONCLUSIONS

1. Forward model showed similar reflectance as simulated by WASI model.
   Similar result was resulting upon simulate the same forward model parameters on WASI model. Therefore the forward model method can be considered correct and the look up table is assumed to derive a correct concentration.
2. Look up table is proven can be used to derived TSM map based on comparison with in situ measurements. A good correlation between derived TSM map concentration and in situ measurements was resulting from the comparison.
3. TSM map derived from MODIS AQUA daily reflectance and MODIS TERRA daily reflectance has close fitting each other with in situ measurements. This is shows that MODIS TERRA and AQUA can be used to derived TSM concentration map.
4. TSM maps derived from LANDSAT 7 ETM and MODIS imageries show large discrepancies.

6.2. RECOMMENDATIONS

1. Look up table script improvements.
   As conclude in this study that the look up table is accurate to derive TSM concentration, this look up table is promising to be applied as a daily water quality monitoring. With the current look up table script applied in this study, look up table implementation requires a long time to complete the implementation. A simplified look up table script is needed to shorten the implementation time in order to be used as a daily water quality observation..
2. More matches up in situ measurement.
   A good correlation was obtained upon comparing in situ measurements with derived TSM maps. However number of the compared in situ measurements point is low. To improve the result confidence, more in situ measurements should be used to test the look up table implementation result.
3. Further study need to be done to investigate the discrepancy between TSM maps derived from LANDSAT ETM and MODIS imageries.

LIST OF REFERENCES

Abu Daya, M. I. (2004). *Coastal water Quality Monitoring with Remote Sensing in East Kalimantan, Makassar Strait, Indonesia.* Unpublished Master of ScienceThesis, ITC, Enschede.

Allen, G. P., & Chambers, J. L. C. (1998). *Sedimentation in the Modern and Miocene Mahakam Delta*: Indonesian Petroleum Association.

Allen, G. P., Laurier, D., & Thouvenin, J. (1976, June). *Sediment Distribution Patterns in The Modern Mahakam Delta.* Paper presented at the 5th Annual Convention of the Indonesian Petroleum Association.

Ambarwulan, W. (2002). *Mapping of TSM Concentrations from SPOT and LANDSAT TM Satellite Images for Integrated Coastal Zone Management in Teluk Banten, Indonesia.* Unpublished Master of Science, ITC, Enschede.

Ambarwulan, W. (2010). *Remote Sensing of Tropical Coastal Waters: Study of The Berau Estuary, East kalimantan, Indonesia* (Vol. 173). Enschede: ITC, University of Twente.

Bappeda Kabupaten Kutai Kartanegara. (2007). *Kutai Kartanegara Dalam Angka 2007. Kutai Kartanegara in Number 2007.*

Bricaud, A., Babin, M., Morel, A., & Claustre, H. (1995). Variability in the Chlorophyll-specific Absorption Coefficients of Natural Phytoplankton: Analysis and Parameterization. *J. Geophys. Res., 100*(C7), 13321-13332.

Bricaud, A., Morel, A., & Prieur, L. (1981). Absorption by Dissolved Organic Matter of the Sea (Yellow Substance) in the UV and Visible domains. *Limnology Oceanography, 26*(1), 11.

Budhiman, S. (2004). *Mapping TSM Concentrations from Multisensor Satellite Images in Turbid Tropical Coastal Waters of Mahakam Delta, Indonesia.* Unpublished Master of Science, ITC, Enschede.

Budhiman, S. (in-preparation). *Quantifying Sediment Fluxes in the Mahakam Delta using Remote Sensing* (Vol. Ph.D.). Enschede Twente University.

Budhiman, S., Salama, M. S., Vekerdy, Z., & Verhoef, W. (in preparation). Deriving Optical Properties of Mahakam Delta Coastal Waters, Indonesia.

Cleveland, J. S. (1995). Regional Models for Phytoplankton Absorption as a Function of Chlorophyll a Concentration. *J. Geophys. Res., 100*(C7), 13333-13344.

D'sa, E. J., & Miller, R. L. (2005). Bio-Optical Properties of Coastal Waters. In R. L. Miller, C. E. D. Castillo & B. A. McKee (Eds.), *Remote Sensing of Coastal Aquatic Environments* (Vol. 7, pp. 129-155). Dordrecht, The Netherlands: Springer.

Davies-Colley, R. J., & Smith, D. G. (2001). Turbidity, Suspended Sediment, and Water Clarity : A Review. *Journal of the American water association, 37-5* 17.

Gege, P. (2004). The water color simulator WASI: an integrating software tool for analysis and simulation of optical in situ spectra. *Computers & Geosciences, 30*(5), 523-532.

Gordon, H. R., Brown, O. B., Evan, R. H., Brown, J. W., Smith, R. C., Baker, K. S., et al. (1988). A Semianalytical Radiance Model of Ocean Color. *Journal of geophysical research, 93(1988)C10, pp. 909-924*.

Gordon, H. R., & Wang, M. (1994). Retrieval of water - leaving radiance and aerosol optical thickness over the oceans with SeaWiFS : a preliminary algorithm. *In: Applied optics, 33(1994)3, pp. 443-452*.

Hellweger, F. L., Schlosser, P., Lall, U., & Weissel, J. K. (2004). Use of satellite imagery for water quality studies in New York Harbor. *Estuarine, Coastal and Shelf Science, 61*(3), 437-448.

Hommerson, A. (2009). A Review on Substances and Processes Relevant for Optical Remote Sensing of Extremely Turbid Marine Areas, with a Focus on the Wadden Sea.

IOCCG. (1998). *Minimum Requirements for An Operational, Ocean-Color Sensor for The Open Ocean* (Report of IOCCG working Group No. 1, 1998). Nova Scotia: International Ocean Colour Coordinating Group.

IOCCG. (2000). *Remote Sensing of Ocean Colour in Coastal, and Other Optically-Complex, Waters*. Dartmouth, Canada: IOCCG.

IOCCG. (2010). *Atmospheric Correction for Remotely-Sensed Ocean Colour Products*. Dartmouth, Canada: IOCCG.

Lee, Z., Carder, K. L., Mobley, C. D., Steward, R. G., & Patch, J. S. (1998). Hyperspectral Remote Sensing for Shallow Waters. I. A Semianalytical Model. *Applied Optics, 37*(27), 10.

Liang, S., Fang, H., & Chen, M. (2001). Atmospheric Correction of Landsat ETM+ Land Surface Imagery-Part I: Methods. *IEEE Transactions on Geoscience and Remote Sensing, 39*(11), 9.

Mandang, I., & Yanagi, T. (2007). Tide and Tidal Current in the Mahakam Estuary, East Kalimantan, Indonesia. *Coastal Marine Science, 32*.

Maritorena, S., Siegel, D. A., & Peterson, A. (2002). Optimization of a Semianalytical Ocean Color Model for Global Scale Applications. *Applied Optics, 41*(15).

Miller, R. L., McKee, B. A., & D'sa, E. J. (2007). Monitoring Bottom Sediment Resuspension and Suspended Sediments in Shallow Coastal Waters. In R. L. Miller, B. A. McKee & E. J. D'sa (Eds.), *Remote Sensing of Coastal Aquatic Environments: Technologies, Techniques and Applications* (Vol. 7, pp. 339). Dordrecht: Springer.

Mobley, C. D. (2004). *Light and Water Radiative Transfer in Natural Waters*: Academic Press.

Morel, A. (1980). In-water and remote measurements of ocean color. *Boundary-Layer Meteorology, 18*(2), 177-201.

NASA. (2008). Landsat 7 Program. *Landsat 7 Science Data Users Handbook* Retrieved 24 August 2010, 2010, from http://landsathandbook.gsfc.nasa.gov/handbook/handbook_htmls/chapter1/chapter1.html

NASA. (2009). The LANDSAT Program. Retrieved 22 August 2010, 2010, from http://landsat.gsfc.nasa.gov/

NASA. (2010). MODIS Web. Retrieved 5 October 2010, 2010, from http://modis.gsfc.nasa.gov/about/specifications.php

NOAA. (2010). WAVEWATCH III Model. from http://polar.ncep.noaa.gov/waves/wavewatch/wavewatch.shtml

Norjamaki, I., & Tokola, T. (2007). Comparison of Atmospheric Correction Methods in Mapping Timber Volume with Multitemporal Landsat Images in kainuu, Finland. *Photogrammetric Engineering & Remote Sensing, 73*(2), 9.

Ouaidrari, H., & Vermote, E. F. (1999). Operational Atmospheric Correction of Landsat TM Data. *Remote Sensing of Environment, 70*(1), 4-15.

Ouillon, S., Douillet, P., Petrenko, A., Neveux, J., dupouy, C., Froidefond, J., et al. (2008). Optical Algorithms at Satellite Wavelengths for Total Suspended Matter in Tropical Coastal Waters. [Open Access]. *Sensors, 8*, 20.

Peel, M. C., Finlayson, B. L., & McMahon, T. A. (2007). Updated world map of the Köppen-Geiger Climate Classification. *Hydrology and Earth System Sciences, 11*, 12.

Pope, R. M., & Fry, E. S. (1997). Absorption Spectrum (380-700 nm) of Pure Water .2. Integrating Cavity Measurements. [Article]. *Applied Optics, 36*(33), 8710-8723.

Pozdnyakov, D., & Grassl, H. (2009). *Colour of Inland and Coastal Waters: A Methodology for Its Interpretation*. German: Springer - Praxis.

Rahman, H., & Dedieu, G. (1994). SMAC: a simplified method for the atmospheric correction of satellite measurements in the solar spectrum. *International Journal of Remote Sensing, 15*(1), 123 - 143.

Robinson, I. S. (1994). *Satellite oceanography : an introduction for oceanographers and remote sensing scientists*. Chichester etc.: Wiley & Sons.

Roesler, C. S., Perry, M. J., & Carder, K. L. (1989). Modeling In Situ Phytoplankton Absorption from Total Absorption Spectra in Productive Inland Marine Waters. *Limnology Oceanography, 34*(8), 24.

Salama, M. S., & F, S. (2009). Simultaneous Atmospheric Correction and Quantification of Suspended Particulate Matters from Orbital and Geostationary Earth Observation Sensors. *Estuarine, Coastal and Shelft Science, 86*(13 October 2009), 13. doi:10.1016/j.ecss.2009.10.001

Sandjatmiko, P. (2006). *Mahakam Delta in Space and Time: Ecosystem, Resources, and Management*. Jakarta: BPMIGAS: TOTAL.

Santoleri, R., Nardelli, B. B., & banzon, V. (2002). Sea Surface Characterization of Combined Data. In F. S. Marzano & G. Visconti (Eds.), *Remote Sensing of Atmosphere and ocean from Space: Models, Instruments and Techniques* (pp. 14).

Sathyendranath, S. (2000). *General Information*. Dartmouth, Canada: IOCCG.

Sidik, A. S. (2009). The Changes of Mangrove Ecdosystem in Mahakam Delta, Indonesia: A Complex Social-Environmental Pattern of Linkage in Resources Utilization. *enaca org*.

Storms, J. E. A., Hoogendoorn, R. M., Dam, R. A. C., Hoitink, A. J. F., & Kroonenberg, S. B. (2005). Late-Holocene evolution of the Mahakam delta, East Kalimantan, Indonesia. *Sedimentary Geology, 180*(3-4), 149-166.

Sturm, B. (1981). The Atmospheric Correction of Remotely Sensed Data and the Quantitative Determination of Suspended Matter in Marine Water Surface Layers. In A. P. Cracknell (Ed.),

Remote Sensing in Meteorology, Oceanography and Hydrology (Vol. 1, pp. 535). West Sussex: Ellis Horwood Limited.

Tian, L., Chen, X., Zhang, T., Gong, W., Chen, L., Lu, J., et al. (2009). Atmospheric correction of ocean color imagery over turbid coastal waters using active and passive remote sensing. *Chinese Journal of Oceanology and Limnology, 27*(1), 124-128.

U.S. Government Public Information Exchange Resource. (2002). The Relative

Spectral Response (RSR) of MODIS. ftp://mcst.hbsss-sigma.com/pub/permanent/MCST/FM1_RSR_LUT_07-10-01/

USGS. (2010, 13 May). Surface Reflectance daily L2G Global 1km and 500m. *LP DAAC*, 2011, from https://lpdaac.usgs.gov/lpdaac/products/modis_products_table/surface_reflectance/daily_l2g_global_1km_and_500m/mod09ga

Vermote, E. F., Kotchenova, S. Y., Roger, J. C., Tanre, D., Deuze, J. L., Herman, M., et al. (2005). Second Simulation of a Satellite Signal in the Solar Spectrum Vector Code (Version 1.0B). Bari, Italy: University of Bari.

Wang, L. T., & DeLiberty, T. L. (2005). *LANDSAT Atmospheric Correction: The Good, The Bad, and The Ugly.* Paper presented at the ESRI.

WeatherUnderground. (1991, 2010). History for Balikpapan, Indonesia. 2010, from http://www.wunderground.com/history/station/96633/2007/1/11/DailyHistory.html?req_city=NA&req_state=NA&req_statename=NA&MR=1

Yu-Hwan Ahn, P. S., Joo-Hyung Ryu. (2004). Atmospheric Correction of The LANDSAT Satellite Imagery For Turbid Waters. *Gayana, 68*(2), 8.

Zaneveld, J. R. V., Twardowski, M. J., Barnard, A., & Lewis, M. R. (2005). Introduction to Radiative Transfer. In R. L. Miller, C. E. D. Castillo & B. A. McKee (Eds.), *Remote Sensing of Coastal Aquatic Environments* (Vol. 7, pp. 1-20). Dordrecht, The Netherlands: Springer.

APPENDIX

APPENDIX A. LANDSAT 7 ETM and MODIS Specification Information

	LANDSAT ETM		MODIS	
Launch Agency	NASA		NASA	
Orbit	Polar, 705 km, 98.2 [deg], 10:00		Polar, 705 km, 98.2 [deg], 10:30 (D, Terra) or 13:30 (A, AQUA)	
Swath	183 km		2330 km	
Quantization	8 bits		12 bits	
Spatial Resolution	30 m (bands 1-5,7); 60 m (band 6); 15-m (band 8)		250 m (bands 1-2); 500 m (bands 3-7); 1000m (bands 8-36)	
Radiometric Accuracy			5% (bands 1-19, 26); 1% (bands 20-25, 27-36)	
Ocean Colour Bands			36: 20 in the VIS and NIR, 10 in the SWIR, and 6 in the LWIR	
	Centre	Width [nm]	Centre [nm]	Width [nm]
			412	15
			443	10
	485	80	488	10
			531	10
	560	80	551	10
	660	80	667	10
			678	10
			748	10
	830		869.5	15

APPENDIX B. Coefficient parameters

Wavelength [nm]	a_w	a_0	a_1
400	0.00663	0.6843	0.0205
410	0.00473	0.7782	0.0129
420	0.004□4	0.8637	0.006
430	□.00495	0.9603	0.002
440	0.00635	1	0
450	0.00922	0.9634	0.006
460	0.00979	0.9311	0.0109
470	0.0106	0.8697	0.0157
480	0.0127	0.789	0.0152
490	0.015	0.7558	0.0256
500	0.0204	0.7333	0.0559
510	0.0325	0.6911	0.0865
520	0.0409	0.6327	0.0981
530	0.0434	0.5681	0.0969
540	0.0474	0.4262	0.0781
550	0.0565	0.3433	0.0659
560	0.0619	0.295	0.06
570	0.0695	0.2784	0.0581
580	0.0896	0.2595	0.054
590	0.1351	0.2389	0.0495
600	0.2224	0.2745	0.0578
610	0.2644	0.3197	0.0674
620	0.2755	0.3421	0.0718
630	0.2916	0.3502	0.0713
640	0.3108	0.561	0.1128
650	0.34	0.8435	0.1595
660	0.41	0.7485	0.1388
670	0.439	0.389	0.0812
680	0.465	0.136	0.0317
690	0.516	0.025	0.005
700	0.624	0.0125	0.0025
710	0.827	0.00625	0.00125
720	1.231	0.003	0.0007
730	1.799	0.001563	0.000313
740	2.38	0.000781	0.000156
750	2.47	0.000391	7.81E-05
760	2.55	0.000195	3.91E-05
770	2.51	9.77E-05	1.95E-05
780	2.36	4.88E-05	9.77E-06
790	2.16	2.44E-05	4.88E-06
800	2.07	1.22E-05	2.44E-06